Cardiovascular Research Advance Access published June 2, 2014

Cardiovascular Research
doi:10.1093/cvr/cvu124

Extent of flow recirculation governs expression of atherosclerotic and thrombotic biomarkers in arterial bifurcations

Jordi Martorell[1,2]*, Pablo Santomá[1,2], Kumaran Kolandaivelu[1], Vijaya B. Kolachalama[1,3], Pedro Melgar-Lesmes[1], José J. Molins[2], Lawrence Garcia[4], Elazer R. Edelman[1,5], and Mercedes Balcells[1,6]

[1]Institute for Medical Engineering and Science, Massachusetts Institute of Technology, Cambridge, MA, USA; [2]Department of Chemical Engineering, IQS School of Engineering, URL, Via Augusta 390, 08017 Barcelona, Spain; [3]Charles Stark Draper Laboratory, Cambridge, MA, USA; [4]Department of Interventional Cardiology and Vascular Medicine, St. Elizabeth's Medical Center, Boston, MA, USA; [5]Cardiovascular Division, Brigham and Women's Hospital and Harvard Medical School, Boston, MA, USA; and [6]Department of Biological Engineering, IQS School of Engineering, URL, Barcelona, Spain

Received 12 December 2013; revised 10 April 2014; accepted 1 May 2014

Time for primary review: 7 days

Aims Atherogenesis, evolution of plaque, and outcomes following endovascular intervention depend heavily on the unique vascular architecture of each individual. Patient-specific, multiscale models able to correlate changes in microscopic cellular responses with relevant macroscopic flow, and structural conditions may help understand the progression of occlusive arterial disease, providing insights into how to mitigate adverse responses in specific settings and individuals.

Methods and results Vascular architectures mimicking coronary and carotid bifurcations were derived from clinical imaging and used to generate conjoint computational meshes for *in silico* analysis and biocompatible scaffolds for *in vitro* models. In parallel with three-dimensional flow simulations, geometrically realistic scaffolds were seeded with human smooth muscle cells (SMC) or endothelial cells and exposed to relevant, physiological flows. *In vitro* surrogates of endothelial health, atherosclerotic progression, and thrombosis were locally quantified and correlated best with an quantified extent of flow recirculation occurring within the bifurcation models. Oxidized low-density lipoprotein uptake, monocyte adhesion, and tissue factor expression locally rose up to three-fold, and phosphorylated endothelial nitric oxide synthase and Krüppel-like factor 2 decreased up to two-fold in recirculation areas. Isolated testing in straight-tube idealized constructs subject to static, oscillatory, and pulsatile conditions, indicative of different recirculant conditions corroborated these flow-mediated dependencies.

Conclusions Flow drives variations in vascular reactivity and vascular beds. Endothelial health was preserved by arterial flow but jeopardized in regions of flow recirculation in a quasi-linear manner. Similarly, SMC exposed to flow were more thrombogenic in large recirculating regions. Health, thrombosis, and atherosclerosis biomarkers correlate with the extent of recirculation in vascular cells lining certain vascular geometries.

Keywords Flow • Endothelium • Geometry • Atherosclerosis • Thrombosis

1. Introduction

Endothelial cells (EC) are exposed to a complex biomechanical milieu and are responsible for relaying biochemical messages to underlying tissue. Disrupted flow patterns[1,2] and, more specifically, flow recirculation exacerbate low-density lipoprotein internalization,[3] cell adhesion molecules expression,[4,5] and monocyte adhesion[6,7] to the endothelium. Such events, in conjunction with other environmental factors,[8] are early determinants for atherosclerosis progression.[9] Though flow disruptions are evident in every vascular bifurcation, their magnitude depend heavily on the geometries specific to every patient and vessel.

The clinical treatment for atherosclerosis has tremendously evolved over many decades, with percutaneous interventions such as stents and/or grafts becoming almost a commodity in patient care.[10] Device deployment, however, creates local, deep injury[11] in the already fragile diseased vessel. Endothelial denudation[12] exposes subintimal smooth

* Corresponding author. Tel: +34 93 267 20 00. Email: jordi.martorell@iqs.edu

muscle cells (SMC) to blood flow, and a cascade of reactions is elicited that modulates vessel patency and may trigger the extrinsic coagulation cascade.

Unravelling the molecular mechanisms behind vascular cell response to physiological and pathological flow characteristics has been for decades a matter of intense research.[13] Both clinical data, obtained with tremendous advances in the field of bioimaging,[8,14–16] and animal models have helped us understand how haemodynamics affect the vessel wall.[17,18] Parallel *in vitro* work[19–21] with idealized bench-top model systems has enabled the cellular and molecular examination of EC biological response to isolated flow descriptors (average flow, maximum amplitude, and flow frequency) in the presence and absence of SMC.

We now test the hypothesis that subtle variations in flow arising in different bifurcation settings are the most powerful predictors of biological markers crucial to our understanding of atherothrombotic disease. We examined how vessel-like, bench-top constructs derived from specific patient geometries create a more precise view of the underlying relationships between flow disruptions and local expressions of atherogenic and thrombotic markers. Using invasive[22] and non-invasive imaging techniques,[23] we reconstructed arterial geometries of different patients for use in a computational model, casted *in vitro* constructs based on the extracted geometry features, and seeded human vascular cells mimicking the arterial wall components. Computational fluid dynamic (CFD) simulations predicted physiological metrics of interest including velocity and quantified regions of flow recirculation. Bench-top-derived measurements of atherogenic and thrombotic markers and their geometry-specific variations were correlated with computational model-based predictions. A scalar metric, defined to capture the extent of recirculation for a specific geometry, correlated with oxidized low-density lipoprotein (Ox-LDL) uptake and localized monocyte adhesion to EC. Furthermore, SMC seeded in regions with a larger extent of recirculation increased their tissue factor (TF) expression. These observations point to the importance of accounting for patient-specific geometry variations and flow derangements to extend derived biological inferences beyond idealized cell culture models to real-world settings.

2. Methods

2.1 Arterial replication platform

Geometrical representations and flow wave forms of the left main coronary artery (LM) bifurcating into left anterior descending (LAD) and left circumflex (LCX) (*Figure 1A* and *D*), and the common carotid artery (CCA) bifurcating into the external (ECA) and internal (ICA) carotid arteries (*Figure 1B* and *E*), were needed as input values for *in silico* and *in vitro* experiments. Design of arterial mimics was performed using a modification of a previously developed computational framework[24] (*Figure 1C*). EC (*Figure 1F*) and SMC (*Figure 1G*) were seeded on polydimethylsiloxane (PDMS) scaffolds. Scanning electron microscopy (SEM) revealed complete cellular coverage along length and circumference of the constructs (*Figure 1H*), and histological examination confirmed multilayer structure of SMC-coated constructs (*Figure 1K*). SMC (*Figure 1I*) and EC (*Figure 1J*) retained their cytoskeletal organization and alignment under flow. Vascular geometries and flow parameters, computational platform design, *in silico* models, and scaffold casting techniques are further detailed in Supplementary material online, Methods.

2.2 Recirculation metrics

The tangential component of the velocity vector (νTan), calculated as the dot product of local velocity vector and normalized direction vector representing the vessel centreline, was used to measure the velocity of the fluid flow (see Supplementary material online, *Figure S2*). This strategy is optimal in curved vessels since it always accounts for local recirculation. Based on νTan, extent of flow recirculation was classified into three categories: severe, mild, or negligible. If maximal backward velocity ($\nu\text{Tan}_{\text{MIN}}$) was above 20% of the inlet velocity during the pulse, extent of recirculation was considered severe. If $\nu\text{Tan}_{\text{MIN}}$ was between 5 and 20%, extent was considered mild, and was negligible if the former criteria were not met. νTan was evaluated at each node and all tetrahedrons containing at least one node with negative νTan were summed to estimate the 'total recirculating volume' (VolRec) for each branch (Eq. 1). The parameter 'normalized νTan·VolRec' (NVV) was calculated multiplying VolRec by νTan, dividing it by the volume of the branch, and normalizing it to the value of the straight segment of the bifurcation (Eq. 2). NVV was the parameter found to best correlate disease biomarkers and flow disruptions (see Supplementary material online, *Figure S3*).

$$\text{VolRec} = \sum(\text{tetrahedrons}_{\nu\text{Tan}<0}) \tag{1}$$

$$\text{NVV} = \frac{\nu\text{Tan} \cdot \text{VolRec/Vol Branch}}{(\nu\text{Tan} \cdot \text{VolRec/Vol Branch})\ \text{Straight Branch}} \tag{2}$$

2.3 Biological assessment of cell-seeded scaffolds

All biological results shown are extracted from the regions of interest. In straight-tube experiments, biomarkers of interest were analysed in the central region of the tube. In bifurcated experiments, data were extracted from the regions of recirculation indicated by CFD simulations (ECA, ICA, LAD, and LCX) and the centre of the straight upstream segments (CCA and LM). All results were normalized to their respective arterial flow (AF) values in single-channel experiments and to the straight sections in the bifurcations.

Vascular cell culture, seeding of scaffolds, perfusion bioreactor, Ox-LDL uptake, monocyte adhesion, vascular cell adhesion molecule 1 (VCAM-1), TF, phosphorylated endothelial nitric oxide synthase (p-eNOS) and Krüppel-like factor 2 (KLF-2) expression, KLF-2 mRNA expression, thrombogenicity, radioimmunoprecipitation assay extraction, western blot analysis, microscopic examination, *ex vivo* detection of macrophage presence in murine carotid bifurcations, and antibodies used are further detailed in Supplementary material online, Methods. All imaging analysis was done using the FIJI imaging platform.[25]

2.4 Human data and samples

All human data (angiographic images) were deidentified, and biological samples (EC, SMC, and blood) were from anonymous donors. Samples and data were treated following the guidelines of the Declaration of Helsinki.

2.5 Statistics

All *in vitro* experiments described were performed on triplicate specimens and repeated two separate times. In graphical presentations, data are expressed as average $\pm$ standard error of mean. Non-parametric Kruskal–Wallis test, followed by a Scheffé *post hoc* analysis of the original measured values normalized to their corresponding controls, was conducted to determine statistical differences between values. Values of $P < 0.05$ were considered statistically significant.

3. Results

3.1 Impact of flow patterns on markers of atherogenesis, and inflammation in EC, and thrombosis in SMC in straight constructs

In our idealized, straight constructs, we observed a protective effect on EC health under conditions of pulsatile unidirectional arterial flow in

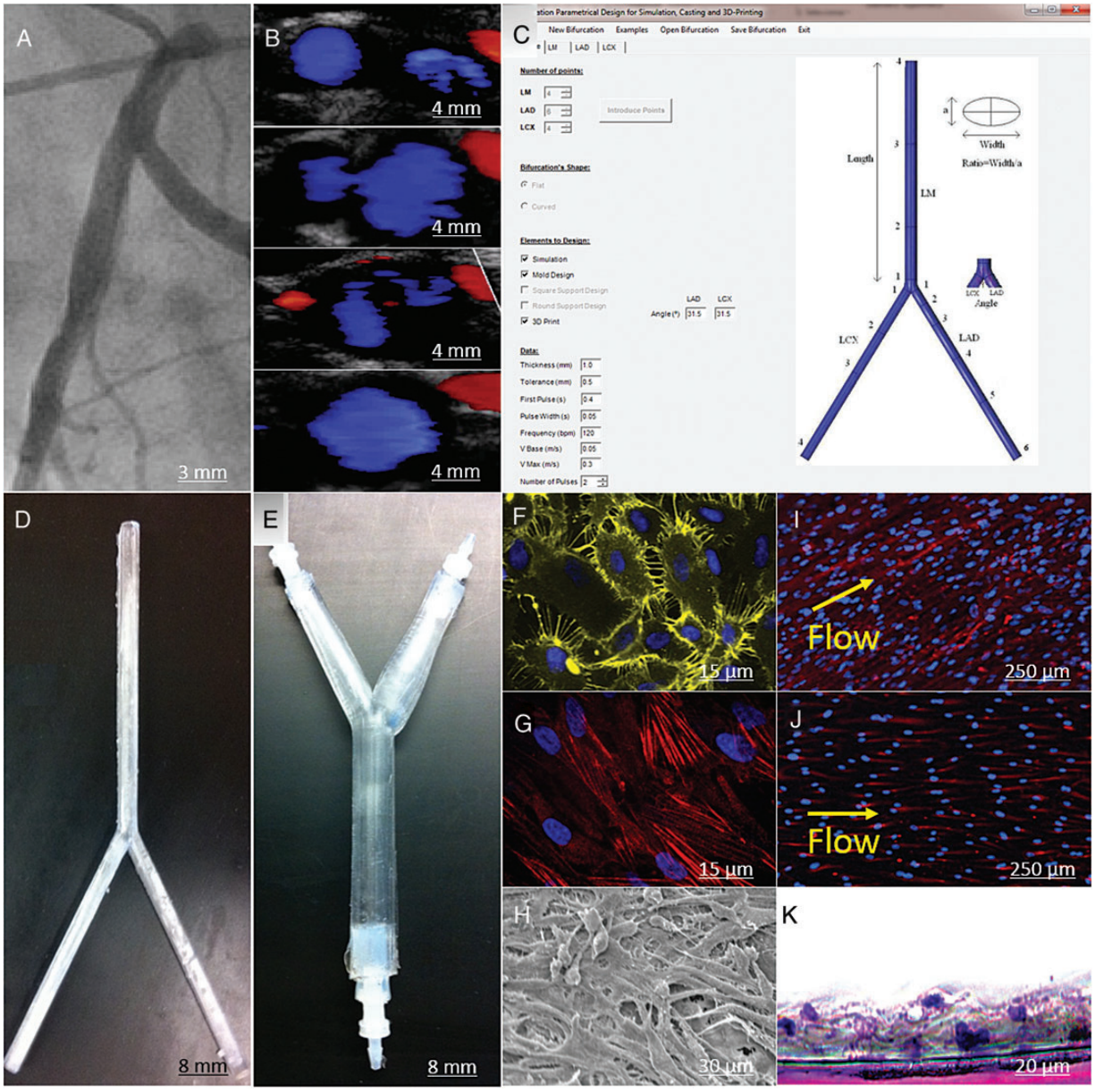

Figure 1 Computational platform to design personalized vessel-like scaffolds. Real data from patients may be obtained with angiographic images (*A*) or eco-Doppler measurements (*B*) and a physician defines the co-ordinates that represent arterial dimensions and that are introduced in a custom-designed Visual Basic® interface (*C*). The interface encodes four different macrofiles for CATIA® that are used to drive formulation of Teflon® moulds that will be used to manufacture PDMS scaffolds (*D* and *E*). A cell-lined tubular structure is created from EC (*F*) [CD31, yellow] or SMC (*G*) [SMC α-actin, red]. Scaffolds were fixed, sputter-coated, and SEM imaged (*H*) or H & E stained (*K*) to confirm seeding homogeneity, coverage, and morphology. SMC (*I*) and EC (*J*) align their tubulin (red) filaments after 24 h exposure to arterial-like flow.

contrast to bidirectional oscillatory flow (OF) and static (STA) conditions. p-eNOS and KLF-2 expression were highest under AF, and were reduced significantly under OF or STA. KLF-2 mRNA expression was also muted in the oscillatory and static cases (data not shown) when compared with the arterial flow case.

VCAM-1 expression (*Figure 2A*), Ox-LDL uptake (*Figure 2C*), and cytokine-induced monocyte adhesion (*Figure 2D*) were highest under oscillatory or static conditions, and were reduced significantly under arterial flow. Activation by tumour necrosis factor alpha (TNF-α) amplified the signal in all cases. The normalized difference in expression of VCAM-1 was muted in activated EC (*Figure 2B*), but Ox-LDL uptake remained lower in the presence of arterial flow even in the face of cytokine stimulation. As expected, monocyte adhesion was below detection limits without TNF-α activation.

Similarly, arterial flow was protective of SMC lacking endothelial shielding. Basal TF levels rose 2.5-fold (*Figure 2G* and *I–K*) under oscillatory flow; in correlation, thrombus formation increased in our model to a similar extent (*Figure 2H* and *L–N*). TF expression by SMC was not affected by TNF-α activation. Thus, not only can disrupted flow exacerbate arterial injury but also the integrity of intact arterial flow may play an important protective role as well.

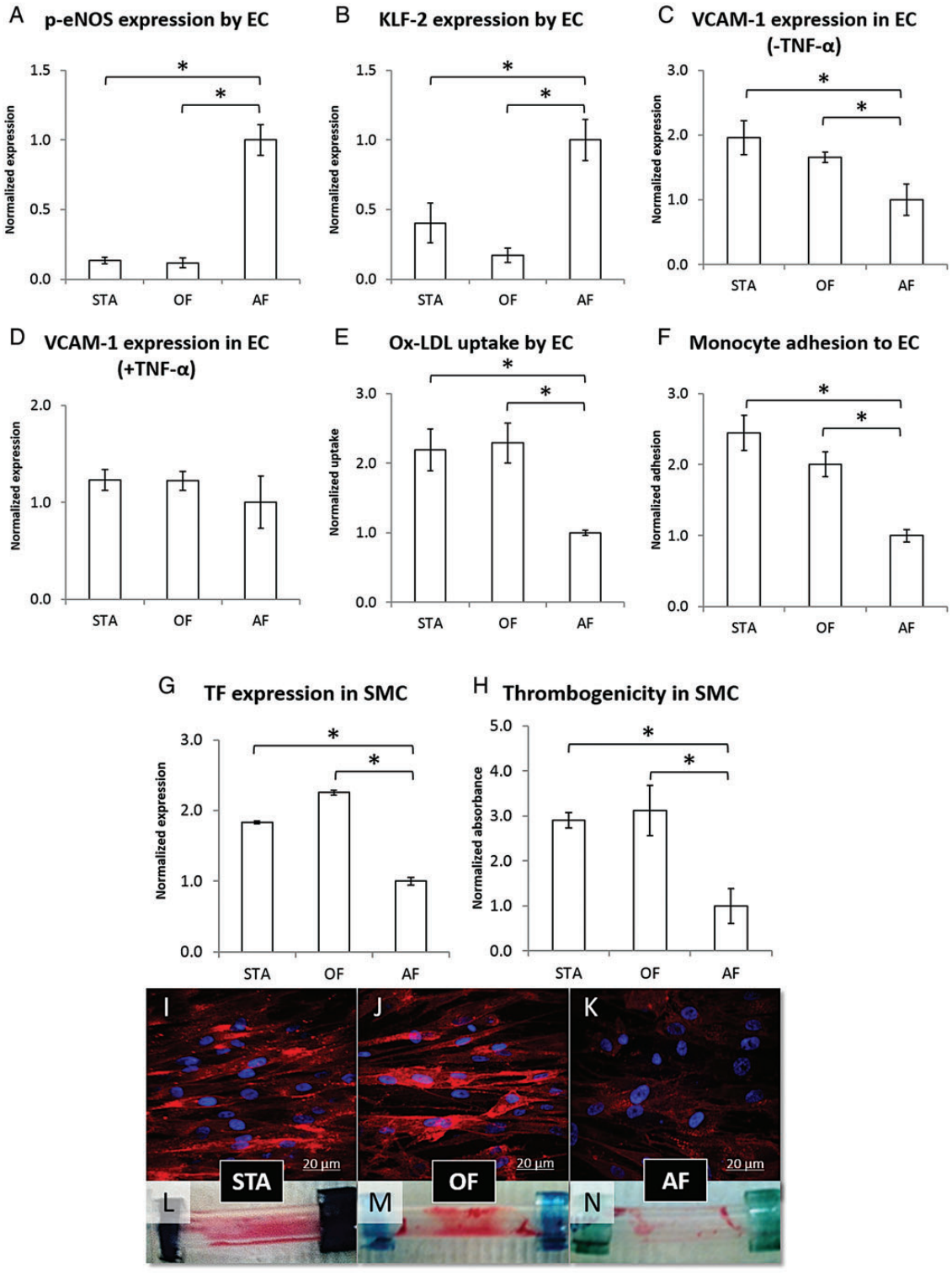

Figure 2 Oscillatory flow jeopardizes vascular health triggering inflammatory response in EC and thrombogenic response in SMC. EC exposed for 24 h to low shear oscillatory flow reduce their p-eNOS (*A*) and KLF-2 (*B*) expression when compared with EC exposed to coronary arterial flow. EC increase VCAM-1 expression when quiescent (*C*), but lose their sensitivity when exposed to inflammatory conditions (*D*). Ox-LDL uptake by EC (*E*) doubled in cells exposed to OF vs. those exposed to AF. Monocyte adhesion to EC (*F*) doubled in cells exposed to OF vs. those exposed to AF under inflammatory conditions. SMC exposed for 24 h to OF up-regulate TF expression by 2.5-fold (*G*) vs. those exposed to AF (*I*–*K*). The previously described[26] thrombogenicity apparatus was used to test SMC after 24 h exposure to AF, OF, or STA (*H*). Thrombogenicity (*L*–*N*) was evaluated as haemoglobin concentration in the cell lysate and increased up to three-fold in SMC exposed to OF, correlating with TF expression. $n = 6$ for each marker described.

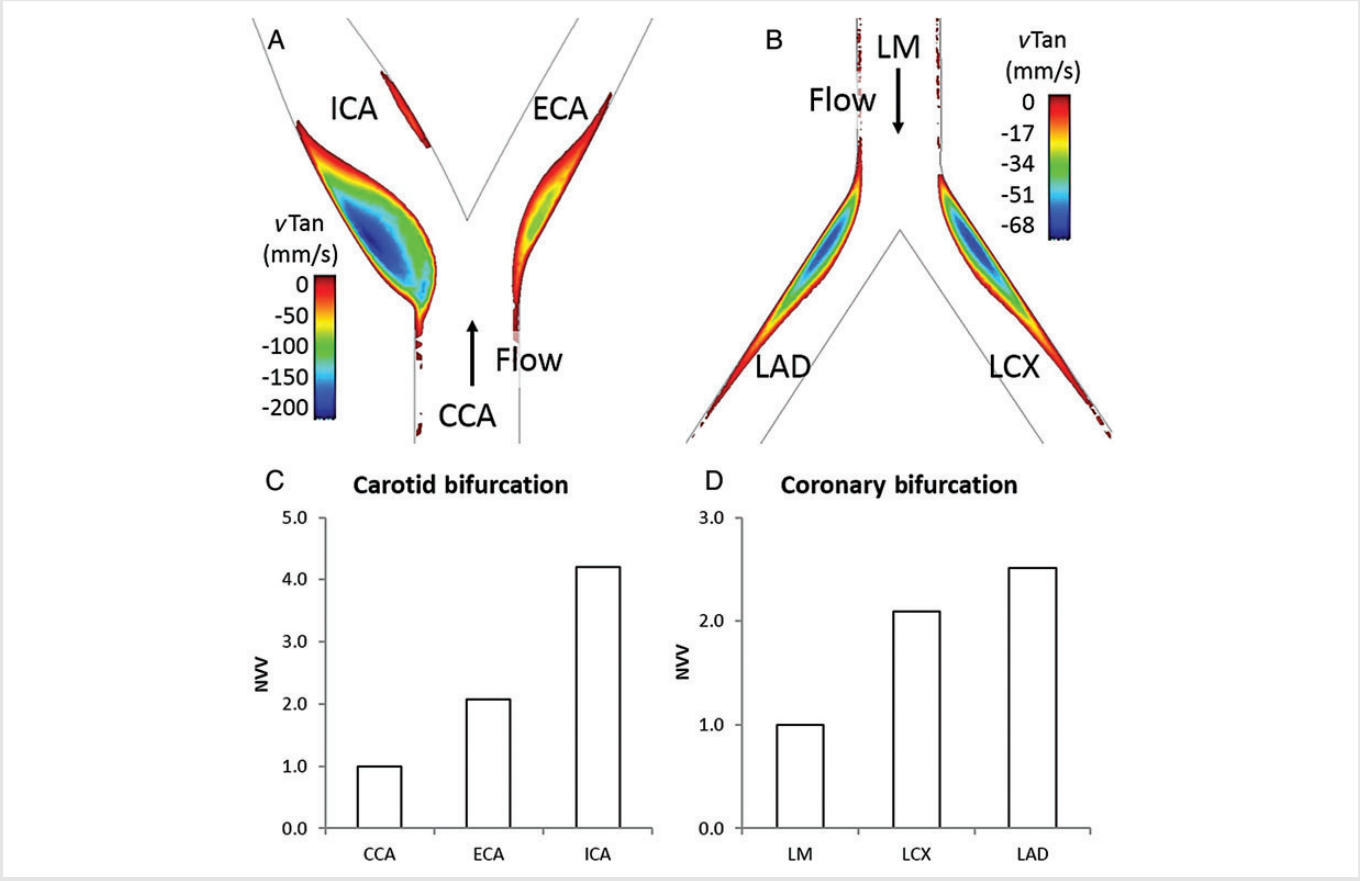

Figure 3 Computational fluid dynamics. Flow recirculations are geometry-dependent. CFD simulations were performed to calculate blood flow profiles in arterial bifurcations. (*A*) The bifurcation of the CCA to the ICA with a minor aneurysm and the ECA. An idealized LM bifurcation into the LAD and LCX (*B*) was also simulated. Results in (*A* and *B*) show negative tangential velocity profiles (νTan) in mm/s at 0.06 s after the pulse. Recirculation areas were observed after a pulse in both branches of each studied bifurcation, with a minimal speed of −195 mm/s for the carotid bifurcation and −65 mm/s for the idealized coronary bifurcation. NVV (*C* and *D*) is measured to establish the correlation between recirculation and disease biomarkers. Recirculation is four-fold (ICA) and two-fold (ECA) more intense than in CCA in the carotid bifurcation (*C*) and about two-fold in the LAD and LCX vs. LM in the coronary bifurcation (*D*).

3.2 Predicting flow patterns in complex geometries

CFD calculations predicted recirculation downstream of bifurcation branches. Recirculation was observed in the two derivative branches of the carotid artery. Severe recirculation ($\nu Tan_{MIN} = -195$ mm/s) was observed in the ICA and mild recirculation ($\nu Tan_{MIN} = -85$ mm/s) in the ECA (*Figure 3A*). The extent of recirculation was four-fold higher in the ICA vs. the CCA (*Figure 3C*), while ECA's increase was around two-fold. An idealized model of the bifurcation of the LM was also studied. The two derivative branches, the LAD and the left circumflex (LCX) branches, presented recirculation that was mild, both in terms of flow reversal (*Figure 3B*) and extent of recirculation (*Figure 3D*). Simulation results were validated by tracking circulating injected latex microparticles.[10]

3.3 Expression of atherogenesis and thrombosis biomarkers correlates with the extent of flow recirculation in arterial bifurcations

Arterial flow appeared to protect EC from inflammatory factors in straight tubes seeded with vascular cells while oscillatory flow (as an idealized model of flow disruption) increased expression of cardiovascular disease biomarkers (*Figure 2*). The same array of tests was run in cell-seeded, 1 : 1 scale bifurcated models (*Figures 4* and *5*).

Phosphorylated eNOS (*Figures 4A* and *5A*) and KLF-2 (*Figures 4B* and *5B*) expression by EC were inversely correlated with NVV, with a 50% reduction for p-eNOS and up to 70% decrease for KLF-2. Contrarily, Ox-LDL uptake by EC (*Figures 4D*, *5D*, see Supplementary material online, *Figure S4A–C*, and *Table 1*), monocyte adhesion to activated EC (*Figures 4E*, *5E*, see Supplementary material online, *Figure S4D–F*, and *Table 1*), and TF expression in SMC (*Figures 4F*, *5F*, see Supplementary material online, *Figure S4G–I*, and *Table 1*) correlated directly, and most powerfully, with the extent of recirculation in each branch of the studied bifurcations.

Ox-LDL uptake by EC increased with the intensity of recirculation, up to three-fold higher than upstream of the bifurcation divider (LM and CCA). Monocyte adhesion to activated EC also grew with the intensity of recirculation, doubling the recruitment by EC free of recirculation. VCAM-1 levels in activated EC, which were blunted in the straight-tube constructs, did not correlate with the observed flow regimes in our bifurcating models (*Figures 4C*, *5C*, and *Table 1*) and were not detectable in the short sections analysed in the absence of TNF-α activation.

In SMC, TF levels were also sensitive to flow recirculation. SMC seeded in areas with severe recirculation showed a 2.5-fold increase in

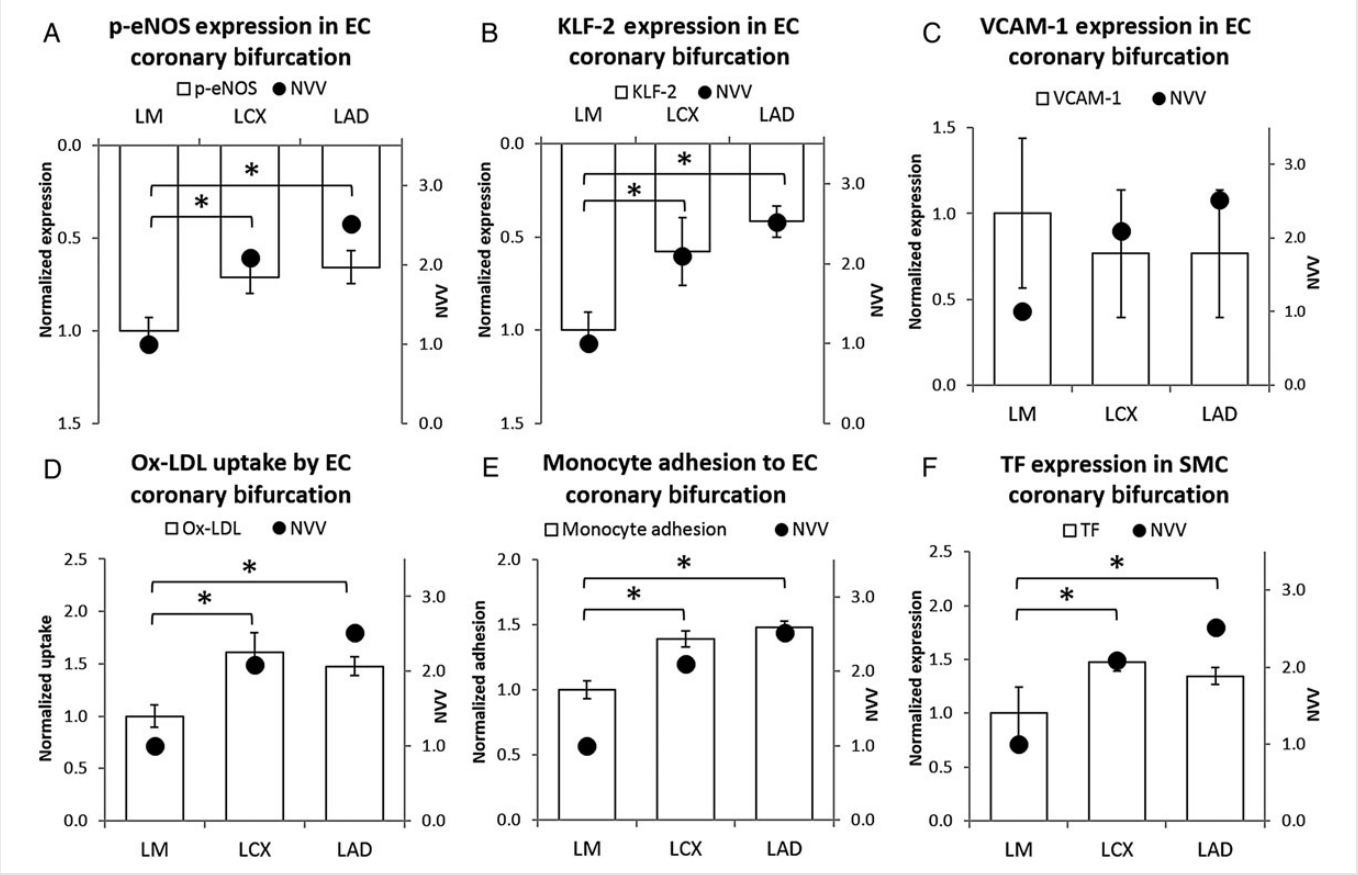

Figure 4 Endothelial inflammatory response and SMC thrombogenic response to geometry-induced flow disruptions in the coronary bifurcation. EC and SMC exposed for 24 h to pulsatile coronary-like flow exhibit different levels of p-eNOS (*A*), KLF-2 (*B*), Ox-LDL uptake (D), monocyte adhesion (*E*), and TF (*F*) as a function of the extent of recirculation in each branch of the coronary bifurcation. p-eNOS and KLF-2 expressions showed significant 40 and 50% respective decreases in regions of recirculation. Ox-LDL uptake by EC had a significant 50% increase for LAD and LCX vs. LM. Similarly, monocyte adhesion in LAD and LCX increased ~40% vs. LM. TF expression in SMC increased in a range between 35 and 50% for LAD and LCX vs. LM. VCAM-1 expression (*C*) was not flow-sensitive. $n = 6$ for each marker described.

TF expression when compared with those seeded in regions exposed to negligible recirculation levels. The presence of macrophage was tested in carotid bifurcations of mice fed with a high-fat diet (see Supplementary material online, *Figure S5*). The extracted carotid geometry was simulated, and regions of flow stagnation near the vessel walls correlated fairly with macrophage recruitment.

4. Discussion

4.1 Flow patterns dictate EC and SMC reactivity

Vascular disease biomarkers and flow patterns are strongly correlated.[5,27–29] In 1983, Zarins *et al.*[27] observed that plaque formed predominantly in regions of flow separation and hypothesized that distinct wall shear stress profiles were responsible for such plaque localization. Dai *et al.*[29] discovered how waveforms could be atheroprotective or atheroprone for EC, and could coexist simultaneously in different regions of the carotid bifurcation. In particular, cDNA array profiling proved that the two waveforms differentially stimulated genes involved in signal transduction, transcriptional regulation, inflammation, angiogenesis, coagulation, and lipid metabolism. They observed how atheroprotective waveforms enhanced KLF-2 and subsequently up-regulated eNOS, while atheroprone waveforms promoted up-regulation of interleukin-8, chemokine receptor type 4, and pentraxin 3 expression, which are biomarkers of atherosclerosis. Disturbed, atheroprone flow regimes usually comprise phases of reversal flow that generate oscillatory wall shear stresses, an attribute notably absent in atheroprotective flow regions.[30] Oscillatory flow has been shown to up-regulate easily detectable cell adhesion molecules such as VCAM-1 or ICAM-1.[31] We chose VCAM-1 as one of the atherogenesis biomarkers instead of ICAM-1, since VCAM-1 seems to be more critical at the beginning of lesion formation.[32] We also chose Ox-LDL uptake and monocyte adhesion, which are fundamental players in atherosclerosis progression.[33] Ox-LDL binds to scavenger receptors CD36[34] and LOX-1,[35] and ligation of LOX-1 induces NF-κB in EC.[36] Transcriptional activation of genes encoding for LDL receptor, with the consequent enhancement of LDL uptake, are increased in EC in disturbed flow regions.[37] Oscillatory flow increases native[38] and Ox-LDL mediated monocyte chemotactic protein-1 expression in EC and subsequent monocyte adhesion.[39] In the same study, high shear stress prevented both Ox-LDL uptake and monocyte adhesion. Depending on the degree of oxidation, LDL induces expression of P-selectin in human umbilical vein endothelial cells, which increases adhesion of monocytes.[6]

The literature is equivocal regarding the effects of haemodynamic forces on the coagulation cascade. While certain groups have reported

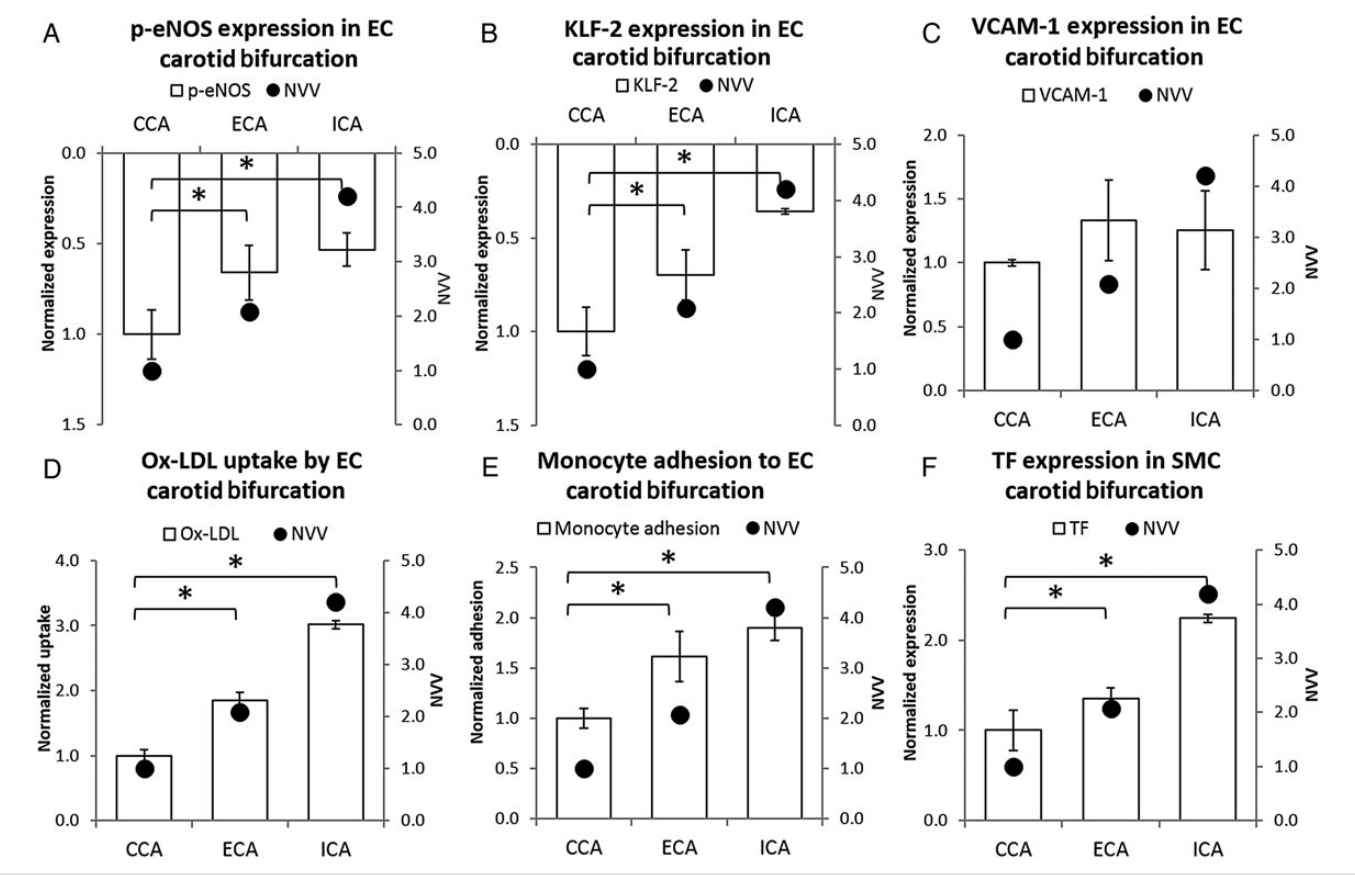

Figure 5 Endothelial inflammatory response and SMC thrombogenic response to geometry-induced flow disruptions in the carotid bifurcation. EC and SMC exposed for 24 h to pulsatile carotid-like flow exhibit different levels of p-eNOS (*A*), KLF-2 (*B*), Ox-LDL uptake (*D*), monocyte adhesion (*E*), and TF (*F*) as a function of the extent of recirculation in each branch of the carotid bifurcation. p-eNOS levels significantly decreased up to 50% and KLF-2 expression was further reduced over 60% in the ICA. Ox-LDL uptake by EC was three-fold higher in the ICA than in the CCA and about two-fold in the ECA. Monocyte adhesion to EC rose two-fold in cells present in the ICA and 1.5-fold in the ECA when compared with the CCA. TD expression in SMC increased about 2.2-fold in the ICA, but a very discrete 1.3-fold in the ECA when compared with CCA. VCAM-1 expression (*C*) was not significantly flow-sensitive. $n = 6$ for each marker described.

Table 1 Comparative biomarkers expression as a function of the extent of recirculation

Recirculation level/ biomarker	Negligible (AF, LM, and CCA)	Mild (LAD, LCX, and ECA)	Severe (ICA)	Oscillatory flow
p-eNOS	↑	↓	↓	↓↓
KLF-2	↑	↓	↓	↓↓
Ox-LDL	=	↑	↑↑	↑↑
Monocyte	=	↑	↑	↑↑
TF	=	↑	↑↑	↑↑
VCAM-1	↑	↑	↑	↑

an increase of TF expression,[40] gene transcription and increased Factor Xa concentration[41] in EC exposed to high shear stress, others affirmed that high shear stress provokes release of the TF pathway inhibitor from EC,[42] reducing TF activity, and hence risk of thrombosis. Other authors reported that TF activity was up-regulated by oscillatory shear stress,[43] and some noted that TF is of only modest importance in EC.[44] While the effects of haemodynamic forces on TF in EC have been deeply explored, the influence of flow on SMC function is poorly characterized.[45] Indeed, the endothelium is denuded after angioplasty[46] and SMC are regularly exposed to blood flow. We therefore exposed single cultures of SMC to pulsatile flow and oscillatory flow along straight tubes and bifurcations, and analysed TF levels to elucidate risk of thrombosis as a function of flow. Although the increase of thrombogenicity may not only be caused by the increase of TF levels, in our system, TF expression in SMC correlated with *ex vivo* clot formation.

4.2 The extent of recirculation simplifies the relationship between geometry and flow and correlates with early markers of EC and SMC diseases

Geometrical and dimensional parameters are often used to define the state of human vasculature[24,27] and link to vascular disease.[47,48] Yet, the number of parameters required to define complex geometries prohibits rigorous characterization and produces a vast array of dimensions

and possible interactions. We propose an alternative strategy that integrates dimensions and physiology into a single flow parameter based on the extent of recirculation in the vessel under study. Instead of limiting the evaluation of risk to a specific number of factors at specific locations in the vessel, we scanned the complete architecture of the vessel tree and determine the risk using a single variable that reflects how geometry affects recirculation. Our data suggest that the distinct geometry of each patient's vascular tree dictates different flow regimes, and that these regimes are the critical players in defining each patient's vascular phenotype. The coronary models, however, did not include the effect of forces caused by the myocardium during systole and diastole. Such forces further increase the oscillatory shear index in the LAD, but do not alter the localization of the recirculation sites.[49]

Indeed, Ox-LDL uptake by EC and monocyte adhesion to activated EC correlated directly with the extent of recirculation in each branch of the studied bifurcations. Furthermore, p-eNOS and KLF-2 expressions were higher in regions of lowest recirculation. The implication of these findings is that endothelial cells function differently when exposed to flows with different levels of recirculation.

The full sequence of atherogenesis was activated in regions of flow recirculation and stagnation. Recirculation was also a powerful predictor of SMC biology where TF expression tracked with the amount of recirculation precisely. In this context, the two elements of the paper come together nicely to explain the power of flow: arterial flow is protective of vascular injury and inductive of repair but subject to disruption by recirculation. Atherosclerosis and thrombosis are, however, highly multifactorial events. The inter-patient variability due to disease progression or after any of a range of vascular interventions can also originate from procedure trauma and release of anti-proliferative drugs, both responsible of potential thrombosis. Micro-recirculations caused at strut level by stent thickness and malapposition also increase the risk of thrombosis.[26] In any case, restoration of flow after a stent deployment should reduce the risk of thrombus linked to blood recirculation.

In vivo correlations between flow recirculation and markers of vascular damage have been established in the past. In 2004, Richter *et al.*[21] proved that regions of recirculation in a porcine model of the iliofemoral bifurcation correlated with leucocyte recruitment and intimal hyperplasia levels. Gimbrone[50] reported analogous findings in murine and rabbit aortic arches in 2010. Very recently, Assemat *et al.*[51] found comparable results correlating *in vivo* atheroma with regions of bidirectional low shear stress in an aortic murine branch calculated by CFD. In this work, we tested the presence of macrophage in carotid bifurcations in mice fed with a high-fat diet. Regions of flow stagnation near the vessel walls were able to predict regions where macrophage recruitment was more dynamic.

4.3 The arterial replication platform is a multidisciplinary tool to study the local impact of flow disruptions

Ever since Gimbrone *et al.* designed the first *in vitro* flow chamber, researchers have tried to find accurate models of arterial flow disruptions. Though precise control over flow and geometry makes these models excellent tools for basic research, these systems do not generally simultaneously expose cells in a single construct to different flow regimes. Single-channel *ex vivo* and *in vitro* models are limited to one flow regime per system and lack the spatial resolution of different regions of a bifurcated artery.

Our system now allows exact replication of vascular architecture,[10] simultaneous exposure of vascular cells to a physiological range of flow regimes within the same construct and quantitative measure of cell- and flow-specific responses. We can examine local recirculation and compare response of genetically identical cells,[2] exposed to the same solutes and <1 cm apart. Cells that might be thought to be identical can now be shown to express significantly different levels of disease biomarkers under the control only of different degrees of recirculation. This spatial control over stimulus is critical in examining the cellular response to local flow alterations. While all inflammation and thrombogenic biomarkers generally rose when cells were exposed to oscillatory flow and static conditions, these values showed a clear correlation with the local extent of recirculation for each branch on each arterial bed. The three-dimensional approach localizes better the impact of flow patterns, but poses novel challenges at the same time. The studied biomarkers presented levels near the detection thresholds of the analytical methods applied, especially in small sections like recirculation regions of the bifurcated constructs.

Integrated frameworks such as the one we described here could be useful in basic research and clinical practice. As an *in vitro* tool, the platform allows for parametrical and mechanistic studies of the impact of patient-specific features in biological outcomes, not only for inflammation or coagulation but also for angiogenesis or cellular migration among many. Our platform has already been proved useful to determine the thrombogenicity and impact of different anti-proliferative treatments on endothelial recovery. The findings might well suggest a different focus in performing procedures—one that focuses on restoration of intact fluid flow rather than where stent struts are located. Increasingly flow is emerging as a quantifiable interventional parameter, and our results will place flow within a greater context. One could even envision extending this work to other flow domains such as the respiratory or urinary tracks.[20] In the future, a parameter such as NVV may be provided to directly guide intervention based on individual patient state and vascular geometry of specific patients to prevent flow- and drug-related post-implantation complications.

4.4 Conclusion

Vascular cells attain a range of phenotypes that are most responsive to their flow environment. Endothelial health is preserved by arterial flow, but jeopardized in regions of flow recirculation in a quasi-linear manner. Similarly, smooth muscle cells exposed to flow are more thrombogenic in large recirculating regions. Thrombotic and inflammatory biomarkers correlate with the extent of recirculation that vascular cells are exposed to when lining certain vascular geometries. The integration of engineering of fluidics with vascular biology is the only means to examine these complex interactions.

Supplementary material

Supplementary material is available at *Cardiovascular Research* online.

Acknowledgements

The authors thank the following people and institutions for their support: Philip Seifert for scanning electronic microscopy and histopathology at CBSET, Nicki Watson and Wendy Salmon for spinning confocal disk microscopy at Whitehead Institute, and Dr Jeffrey Wyckoff for multiphoton imaging at Koch Institute. We also acknowledge Dr Caroline C. O'Brien, Dr Vipul Chitalia, Dr Andrés A. García-Granada, Jay

Wang, Elisabet Rosàs, and Fernando García-Polite for their technical support and intellectual discussion.

Conflict of interest: none declared.

Funding

This work was supported by the National Institute of Health/National Institute of General Medical Science (RO1/GM049039 to E.R.E.); Ministerio de Ciencia e Innovación (BFU 2009-09804 to M.B., J.J.M., and E.R.E.); MIT International Science and Technology Initiatives (MIT-Spain Seed Fund 2010 to E.R.E. and J.J.M.); Generalitat de Catalunya (2013FI_B2 00093 to J.M. and MOBINT 2011 to P.S.), Banco Santander (Fórmula Santander 2011 to P.S.) and POSIMAT (PS2010-2013 to M.B.).

References

1. Richter Y, Edelman ER. Cardiology is flow. *Circulation* 2006;**113**:2679–2682.
2. Chiu JJ, Chien S. Effects of disturbed flow on vascular endothelium: pathophysiological basis and clinical perspectives. *Physiol Rev* 2011;**91**:327–387.
3. Phelps JE, DePaola N. Spatial variations in endothelial barrier function in disturbed flows in vitro. *Am J Physiol Heart Circ Physiol* 2000;**278**:H469–H476.
4. Chiu JJ, Chen LJ, Lee PL, Lee CI, Lo LW, Usami S, Chien S. Shear stress inhibits adhesion molecule expression in vascular endothelial cells induced by coculture with smooth muscle cells. *Blood* 2003;**101**:2667–2674.
5. Methe H, Balcells M, Alegret Mdel C, Santacana M, Molins B, Hamik A, Jain MK, Edelman ER. Vascular bed origin dictates flow pattern regulation of endothelial adhesion molecule expression. *Am J Physiol Heart Circ Physiol* 2007;**292**:H2167–H2175.
6. Gleissner CA, Leitinger N, Ley K. Effects of native and modified low-density lipoproteins on monocyte recruitment in atherosclerosis. *Hypertension* 2007;**50**:276–283.
7. Gleissner CA, Ley K. Cxcl4 in atherosclerosis: possible roles in monocyte arrest and macrophage foam cell formation. *Thromb Haemost* 2007;**98**:917–918.
8. Rudd JH, Myers KS, Bansilal S, Machac J, Woodward M, Fuster V, Farkouh ME, Fayad ZA. Relationships among regional arterial inflammation, calcification, risk factors, and biomarkers: a prospective fluorodeoxyglucose positron-emission tomography/computed tomography imaging study. *Circ Cardiovasc Imaging* 2009;**2**:107–115.
9. Koskinas KC, Feldman CL, Chatzizisis YS, Coskun AU, Jonas M, Maynard C, Baker AB, Papafaklis MI, Edelman ER, Stone PH. Natural history of experimental coronary atherosclerosis and vascular remodeling in relation to endothelial shear stress: a serial, in vivo intravascular ultrasound study. *Circulation* 2010;**121**:2092–2101.
10. Martorell J, Santoma P, Molins JJ, Garcia-Granada AA, Bea JA, Edelman ER, Balcells M. Engineered arterial models to correlate blood flow to tissue biological response. *Ann N Y Acad Sci* 2012;**1254**:51–56.
11. Rogers C, Tseng DY, Squire JC, Edelman ER. Balloon-artery interactions during stent placement: a finite element analysis approach to pressure, compliance, and stent design as contributors to vascular injury. *Circ Res* 1999;**84**:378–383.
12. Douglas G, Van Kampen E, Hale AB, McNeill E, Patel J, Crabtree MJ, Ali Z, Hoerr RA, Alp NJ, Channon KM. Endothelial cell repopulation after stenting determines in-stent neointima formation: effects of bare-metal vs. drug-eluting stents and genetic endothelial cell modification. *Eur Heart J* 2013;**34**:3378–3388.
13. Davies PF. Hemodynamic shear stress and the endothelium in cardiovascular pathophysiology. *Nat Clin Pract Cardiovasc Med* 2009;**6**:16–26.
14. Dumont DM, Doherty JR, Trahey GE. Noninvasive assessment of wall-shear rate and vascular elasticity using combined ARFI/SWEI/spectral Doppler imaging system. *Ultrason Imaging* 2011;**33**:165–188.
15. Lee MY, Wu CM, Yu KH, Chu CS, Lee KT, Sheu SH, Lai WT. Association between wall shear stress and carotid atherosclerosis in patients with never treated essential hypertension. *Am J Hypertens* 2009;**22**:705–710.
16. Waxman S, Freilich MI, Suter MJ, Shishkov M, Bilazarian S, Virmani R, Bouma BE, Tearney GJ. A case of lipid core plaque progression and rupture at the edge of a coronary stent: elucidating the mechanisms of drug-eluting stent failure. *Circ Cardiovasc Interv* 2010;**3**:193–196.
17. Dolan JM, Kolega J, Meng H. High wall shear stress and spatial gradients in vascular pathology: a review. *Ann Biomed Eng* 2013;**41**:1411–1427.
18. Tremmel M, Xiang J, Hoi Y, Kolega J, Siddiqui AH, Mocco J, Meng H. Mapping vascular response to in vivo hemodynamics: application to increased flow at the basilar terminus. *Biomech Model Mechanobiol* 2010;**9**:421–434.
19. Blackman BR, Garcia-Cardena G, Gimbrone MA Jr. A new in vitro model to evaluate differential responses of endothelial cells to simulated arterial shear stress waveforms. *J Biomech Eng* 2002;**124**:397–407.
20. Balcells M, Martorell J, Olive C, Santacana M, Chitalia V, Cardoso AA, Edelman ER. Smooth muscle cells orchestrate the endothelial cell response to flow and injury. *Circulation* 2010;**121**:2192–2199.
21. Richter Y, Groothuis A, Seifert P, Edelman ER. Dynamic flow alterations dictate leukocyte adhesion and response to endovascular interventions. *J Clin Invest* 2004;**113**:1607–1614.
22. Schonenberger E, Schnapauff D, Teige F, Laule M, Hamm B, Dewey M. Patient acceptance of noninvasive and invasive coronary angiography. *PLoS ONE* 2007;**2**:e246.
23. Hozumi T, Yoshida K, Akasaka T, Asami Y, Ogata Y, Takagi T, Kaji S, Kawamoto T, Ueda Y, Morioka S. Noninvasive assessment of coronary flow velocity and coronary flow velocity reserve in the left anterior descending coronary artery by Doppler echocardiography: comparison with invasive technique. *J Am Coll Cardiol* 1998;**32**:1251–1259.
24. Kolachalama VB, Bressloff NW, Nair PB. Mining data from hemodynamic simulations via bayesian emulation. *Biomed Eng Online* 2007;**6**:47.
25. Schindelin J, Arganda-Carreras I, Frise E, Kaynig V, Longair M, Pietzsch T, Preibisch S, Rueden C, Saalfeld S, Schmid B, Tinevez JY, White DJ, Hartenstein V, Eliceiri K, Tomancak P, Cardona A. Fiji: an open-source platform for biological-image analysis. *Nat Methods* 2012;**9**:676–682.
26. Kolandaivelu K, Swaminathan R, Gibson WJ, Kolachalama VB, Nguyen-Ehrenreich KL, Giddings VL, Coleman L, Wong GK, Edelman ER. Stent thrombogenicity early in high-risk interventional settings is driven by stent design and deployment and protected by polymer-drug coatings. *Circulation* 2011;**123**:1400–1409.
27. Zarins CK, Giddens DP, Bharadvaj BK, Sottiurai VS, Mabon RF, Glagov S. Carotid bifurcation atherosclerosis. Quantitative correlation of plaque localization with flow velocity profiles and wall shear stress. *Circ Res* 1983;**53**:502–514.
28. Hamik A, Lin Z, Kumar A, Balcells M, Sinha S, Katz J, Feinberg MW, Gerzsten RE, Edelman ER, Jain MK. Kruppel-like factor 4 regulates endothelial inflammation. *J Biol Chem* 2007;**282**:13769–13779.
29. Dai G, Kaazempur-Mofrad MR, Natarajan S, Zhang Y, Vaughn S, Blackman BR, Kamm RD, Garcia-Cardena G, Gimbrone MA Jr. Distinct endothelial phenotypes evoked by arterial waveforms derived from atherosclerosis-susceptible and -resistant regions of human vasculature. *Proc Natl Acad Sci USA* 2004;**101**:14871–14876.
30. Davies PF, Civelek M, Fang Y, Fleming I. The atherosusceptible endothelium: endothelial phenotypes in complex haemodynamic shear stress regions in vivo. *Cardiovasc Res* 2013;**99**:315–327.
31. Chappell DC, Varner SE, Nerem RM, Medford RM, Alexander RW. Oscillatory shear stress stimulates adhesion molecule expression in cultured human endothelium. *Circ Res* 1998;**82**:532–539.
32. Cybulsky MI, Iiyama K, Li H, Zhu S, Chen M, Iiyama M, Davis V, Gutierrez-Ramos JC, Connelly PW, Milstone DS. A major role for VCAM-1, but not ICAM-1, in early atherosclerosis. *J Clin Invest* 2001;**107**:1255–1262.
33. Dansky HM, Barlow CB, Lominska C, Sikes JL, Kao C, Weinsaft J, Cybulsky MI, Smith JD. Adhesion of monocytes to arterial endothelium and initiation of atherosclerosis are critically dependent on vascular cell adhesion molecule-1 gene dosage. *Arterioscler Thromb Vasc Biol* 2001;**21**:1662–1667.
34. Kopprasch S, Pietzsch J, Westendorf T, Kruse HJ, Grassler J. The pivotal role of scavenger receptor cd36 and phagocyte-derived oxidants in oxidized low density lipoprotein-induced adhesion to endothelial cells. *Int J Biochem Cell Biol* 2004;**36**:460–471.
35. Li D, Mehta JL. Antisense to LOX-1 inhibits oxidized LDL-mediated upregulation of monocyte chemoattractant protein-1 and monocyte adhesion to human coronary artery endothelial cells. *Circulation* 2000;**101**:2889–2895.
36. Rajavashisth TB, Yamada H, Mishra NK. Transcriptional activation of the macrophage-colony stimulating factor gene by minimally modified LDL. Involvement of nuclear factor-kappa β. *Arterioscler Thromb Vasc Biol* 1995;**15**:1591–1598.
37. Liu Y, Chen BP, Lu M, Zhu Y, Stemerman MB, Chien S, Shyy JY. Shear stress activation of SREBP1 in endothelial cells is mediated by integrins. *Arterioscler Thromb Vasc Biol* 2002;**22**:76–81.
38. Hsiai TK, Cho SK, Wong PK, Ing M, Salazar A, Sevanian A, Navab M, Demer LL, Ho CM. Monocyte recruitment to endothelial cells in response to oscillatory shear stress. *FASEB J* 2003;**17**:1648–1657.
39. Hsiai TK, Cho SK, Reddy S, Hama S, Navab M, Demer LL, Honda HM, Ho CM. Pulsatile flow regulates monocyte adhesion to oxidized lipid-induced endothelial cells. *Arterioscler Thromb Vasc Biol* 2001;**21**:1770–1776.
40. Rochier A, Nixon A, Yamashita N, Abe R, Abe R, Madri JA, Sumpio BE. Laminar shear, but not orbital shear, has a synergistic effect with thrombin stimulation on tissue factor expression in human umbilical vein endothelial cells. *J Vasc Surg* 2011;**54**:480–488.
41. Lin MC, Almus-Jacobs F, Chen HH, Parry GC, Mackman N, Shyy JY, Chien S. Shear stress induction of the tissue factor gene. *J Clin Invest* 1997;**99**:737–744.
42. Grabowski EF, Reininger AJ, Petteruti PG, Tsukurov O, Orkin RW. Shear stress decreases endothelial cell tissue factor activity by augmenting secretion of tissue factor pathway inhibitor. *Arterioscler Thromb Vasc Biol.* 2001;**21**:157–162.
43. Mazzolai L, Silacci P, Bouzourene K, Daniel F, Brunner H, Hayoz D. Tissue factor activity is upregulated in human endothelial cells exposed to oscillatory shear stress. *Thromb Haemost* 2002;**87**:1062–1068.
44. Osterud B, Bjorklid E. Sources of tissue factor. *Semin Thromb Hemost* 2006;**32**:11–23.
45. Ekstrand J, Razuvaev A, Folkersen L, Roy J, Hedin U. Tissue factor pathway inhibitor-2 is induced by fluid shear stress in vascular smooth muscle cells and affects cell proliferation and survival. *J Vasc Surg* 2010;**52**:167–175.
46. Bates ER, McGillem MJ, Beals TF, DeBoe SF, Mikelson JK, Mancini GB, Vogel RA. Effect of angioplasty-induced endothelial denudation compared with medial injury on regional coronary blood flow. *Circulation* 1987;**76**:710–716.
47. VanderLaan PA, Reardon CA, Getz GS. Site specificity of atherosclerosis: site-selective responses to atherosclerotic modulators. *Arterioscler Thromb Vasc Biol* 2004;**24**:12–22.

48. Iiyama K, Hajra L, Iiyama M, Li H, DiChiara M, Medoff BD, Cybulsky MI. Patterns of vascular cell adhesion molecule-1 and intercellular adhesion molecule-1 expression in rabbit and mouse atherosclerotic lesions and at sites predisposed to lesion formation. *Circ Res* 1999;**85**:199–207.
49. Ramaswamy SD, Vigmostad SC, Wahle A, Lai YG, Olszewski ME, Braddy KC, Brennan TM, Rossen JD, Sonka M, Chandran KB. Fluid dynamic analysis in a human left anterior descending coronary artery with arterial motion. *Ann Biomed Eng* 2004;**32**:1628–1641.
50. Gimbrone MA. The Gordon Wilson lecture. Understanding vascular endothelium: a pilgrim's progress. Endothelial dysfunction, biomechanical forces and the pathobiology of atherosclerosis. *Trans Am Clin Climatol Assoc* 2010;**121**:115–127. discussion 127.
51. Assemat P, Armitage JA, Siu KK, Contreras KG, Dart A, Chin-Dusting J, Hourigan K. Three-dimensional numerical simulation of blood flow in mouse aortic arch around atherosclerotic plaques. *Appl Math Model.* 2014; doi: http://dx.doi.org/10.1016/j.apm.2014.01.004.

SUPPLEMENTAL METHODS

Vascular geometries and flow parameters

A representation of coronary and carotid geometries and flow wave forms was needed as input values for *in silico* and *in vitro* experiments. When available, such values were taken from published data, or otherwise, measured. De-identified DICOM images of angiograms from patients undergoing coronary angiography/angioplasty for primary medical indication(s) were used to create the coronary artery models under a protocol approved by the Institutional Review Board at St. Elizabeth's Medical Center in Boston. Blood flow wave form and center line peak were extracted from previously published data[1]. Geometric parameters for the carotid model were obtained from previously published data[2] (Figure 1E, Table S1B). The velocities in the different branches of the carotid bifurcation were obtained using Doppler echography on healthy volunteers (Figure 1B). All straight tube controls had the same diameter as the idealized left main coronary artery (3.6mm).

Computational platform

Design of the arterial mimics was performed using a modification of a previously developed computational framework[3]. The interface encodes up to four different macro files for Catia® (Figure 1C). An IGS file is the bridge to computational fluid dynamics (CFD) calculations in Tdyn®. CAM files drive the computer numerical control mechanization of Teflon® (Broncesval, Barcelona, Spain) molds. Straight vessel-like constructs were cut and prepared as previously described.[4] For bifurcated geometries (Figure 1D-E), biologically inert polydimethylsiloxane (PDMS, Dow Corning, Midland, MI) was chosen.

In silico models

Computational simulations were performed using a finite volume solver (Tdyn®)[5]. Arterial blood flow was simulated through geometries of human coronary bifurcations and human and murine carotid bifurcations. For human blood, fluid was assumed to be incompressible and Newtonian with a density of 1035 kg/m^3 and a viscosity of 0.0035 Pa·s. A parabolic velocity was applied normal to the inlet surface that was pulsatile in nature, and scaled for a peak systolic velocity of

0.7 m/s for the carotid bifurcation and 0.35 m/s for the coronary bifurcations model, identical to the profiles set to the bench-top perfusion bioreactor. Simulations were run using blood flow wave form and center line peak extracted from healthy volunteers for two pulses at 1Hz with a time increment of 0.5 ms/step. For murine carotid models, fluid was assumed to be incompressible and Newtonian with a density of 1057 kg/m^3 and a viscosity of 0.00134 Pa·s [6]. A parabolic velocity was applied normal to the inlet surface that was pulsatile in nature, and scaled for a peak systolic velocity of 0.75 m/s. Simulations were run using blood flow wave form and center line peak extracted from published data [7] for two pulses at 5Hz with a time increment of 0.4 ms/step. The walls were considered rigid and the outlet was defined with a zero pressure condition. The geometries were spatially discretized to yield an unstructured tetrahedral mesh with maximal edge length ranging between 0.2 and 0.7 mm in human models and between 0.0003 and 0.0005 mm for a total of 117,000 nodes for the human carotid bifurcation, 108,000 nodes in the human coronary bifurcation and 60,000 in the murine model. These node counts yielded a mesh independent solution for the studied variables. Laminar flow assumption was used since Re≈850 in the human carotid bifurcation, Re≈450 in the human coronary bifurcation and Re≈55 in the murine carotid bifurcation.

Construct casting

In a first step, two positive Teflon® molds of the bifurcation were machined using a computer numeric control machine Fagor® 8055 (Fagor, Mondragon, Spain). Consequently, liquid polyurethane (Smooth-On, Easton, PA) was poured on the top of the two molds to obtain, after 16h curing, two flexible PU negative molds. The polyurethane molds were assembled to create a cavity identical to the desired bifurcation. A pre-warmed (70^0C) optical soluble wax (Universal Photonics, Hicksville, NY) was injected through the cavity and cooled down until room temperature to obtain the solid core that would allow generation of the bifurcation lumen. Thereafter, liquid PDMS was poured in a Teflon® tray, where the silicone would polymerize following both the core and the tray shape. Finally, the solid wax core was dissolved in hot water (80^0C) for 2 hours. After 20 minutes cleaning with 0.2% sodium dodecyl sulfate in distilled water and two consecutive rinses with distilled water, the hollow bifurcated construct was autoclaved at 120^0C and 2 bar.

Vascular cell culture

Human coronary artery endothelial cells (EC) (Promocell, Heidelberg, Germany) were cultured in EBM-2 basal medium (Lonza) supplemented with 7% fetal bovine serum, 1% penicillin-streptomycin, 0.04% hydrocortisone, 0.4% hFGF-B, 0.1% VEGF, 0.1% R3-IGF-1, 0.1% ascorbic acid, 0.1% hEGF, and 0.1% GA-1000 (EGM-2). Human aortic smooth muscle cells (SMC, ATCC, Manassas, VA) were cultured with Low Glucose DMEM (Life Technologies, Carlsbad, CA) supplemented with 5% calf serum, 1% glutamine, and 1% penicillin-streptomycin. Cells were fed every 48h, and incubated at 37ºC and 5% CO_2 in a humidified incubator. Experiments were performed using cells in passages ranging from passage 4 to 6.

Seeding of constructs

The straight and bifurcated constructs were coated with 150µg/ml fibronectin (Sigma, St. Louis, MO) in phosphate buffer saline (PBS, Lonza, Allendale, NJ) overnight at 4ºC and washed once to remove loosely adsorbed fibronectin. SMC and EC cultures were maintained as detailed in the supplemental methods. SMC or EC ($1 \cdot 10^6$ cells/mL) were seeded on the fibronectin-coated constructs and remained under axial rotation (10rph) for 48h. Using immunofluorescence (IF), EC were identified with CD31 staining (Figure 1F) and SMC via α-SMC-actin identification (Figure 1G). SEM revealed complete cellular coverage along the length and the circumference of the constructs (Figure 1H) and histological examination confirmed the multilayer structure of SMC-coated constructs (Figure 1K). SMC (Figure 1I) and EC (Figure 1J) retained their cytoskeletal organization and alignment under flow as seen by alpha-tubulin immunostaining.

Perfusion bioreactor

Straight and bifurcated constructs were connected to the perfusion bioreactor as previously described[4] and the constructs exposed to controlled flow of defined media (Video S1). Straight tubes were exposed to coronary artery–like flow (AF), oscillatory flow (OF) or static condition (STA). STA was used as an approximation to regions of partial flow stagnation in a bifurcation. AF was 1Hz parabolic pulsatile flow with centerline peak velocity of 0.35 m/s and was used as

an idealization of blood flowing through the straight, upstream section of a bifurcation. OF, a 1Hz parabolic oscillatory flow with centerline peak velocity of 0.10 m/s, approximated blood recirculating in the regions downstream of the bifurcations.[8-10] In the coronary bifurcation model, media entered the main branch at 1Hz parabolic pulses with center line peak velocity of 0.35 m/s. In the carotid model, flow entered the bifurcation at 1Hz parabolic pulses with center line peak velocity of 0.70 m/s.

Animal studies

Male C57BL/6 mice (The Jackson Laboratory, Bar Harbor, ME). Animals were maintained in a temperature-controlled room (22°C) on a 12-h light-dark cycle. The study was approved by the Animal Ethics Committee at Massachusetts Institute of Technology. After arrival, mice were continuously fed with a high-fat diet (60% fat diet, Research Diets, New Brunswick, NJ) for 10 weeks until the imaging procedure described later. Euthanasia was performed by overexposure to CO_2.

p-eNOS and KLF-2 expression

For p-eNOS and KLF-2 expression in EC, constructs were perfused with EGM-2 medium for 24h. After that, constructs were cut by regions of interest, cells were lysed using RIPA and Western blots were run.

Oxidized Low Density Lipoproteins (Ox-LDL) uptake

EC were perfused with EGM-2 supplemented with 7.5 µg/mL Dil-Ox-LDL (Biomedical Technologies, Stoughton, MA) for 24h. Thereafter, tubes were rinsed with PBS, fixed with paraformaldehyde, stained with DAPI and imaged at 405nm and 560nm. The Ox-LDL content in EC was evaluated by quantifying the Dil intensity of the obtained IF images.

VCAM-1 expression

For VCAM-1 expression in EC, tumor necrosis alpha (TNF-α, Sigma) was added to increase the signal to noise ratio. The constructs were perfused with EGM-2 medium supplemented with 3

ng/mL of TNF-α for 24h. After that, the constructs were cut by regions of interest, cells were lysed using radioimmunoprecipitation assay (RIPA) and Western blots were run.

Monocyte adhesion

EC within the constructs were perfused with medium supplemented with TNF-α for 24h to mimic the vascular inflammatory milieu. Primary monocytes were separated before each assay from blood drawn from healthy male subjects (Blood Research Components, Cambridge, MA), and separated using a negative isolation method (Miltenyi Biotec, Auburn, CA). Monocyte separation yield was confirmed as previously described[11, 12]. Isolated monocytes were injected in the constructs at a 1:1 monocyte/EC ratio and incubated under axial rotation at 37ºC and 5% CO_2 for 2 hours. Thereafter, tubes were rinsed with PBS, fixed and stained for α-tubulin and DAPI. Fluorescent images were obtained at 405nm and 640nm. The ratio of adherent monocytes was quantified by analyzing the obtained IF images.

Tissue factor (TF) expression

For TF expression in SMC, constructs were perfused with EGM-2. After flow exposure, the constructs were stained for TF and DAPI and imaged following the IF protocol (supplemental methods).

KLF-2 mRNA expression

Total RNA from cultured cells was extracted using RNeasy Kits (Life Technologies). 1 µg aliquots of total RNA were reverse transcribed using a complementary High-Capacity cDNA Reverse Transcription Kit (Life Technologies). Primers and probes for gene expression assays were KLF-2 (Taqman assay reference from Life Technologies: Hs00360439_g1), and Taqman Pre-developed Assay Human GAPDH (Life Technologies) as endogenous control. Expression assays were designed using the Taqman Gene Expression assay software (Life Technologies). Real-time quantitative polymerase chain reaction (RT-PCR) was analyzed in duplicate and performed with a Lightcycler-480 (Roche Diagnostics, Basel, Switzerland). 10 µl aliquots of the total volume reaction of 1:8 cDNA dilutions, Taqman probe and primers and FastStart TaqMan Master (Life Technologies) were used in each RT-PCR. The fluorescence signal was captured during each of

the 45 cycles (denaturing 10s at 95 C, annealing 15s at 60 C and extension 20s at 72 C). Water was used as a negative control. Relative quantification was calculated using the comparative threshold cycle (CT), which is inversely related to the abundance of mRNA transcripts in the initial sample. The mean CT of duplicate measurements was used to calculate ΔCT as the difference in CT for target and reference. The relative quantity of the product was expressed as fold induction of the target gene compared with the control primers according to the formula 2-ΔΔCT, where ΔΔCT represents ΔCT values normalized with the mean ΔCT of control samples

Thrombogenicity

After 24 hours of in the perfusion bioreactor, straight constructs were explanted and gently flushed to remove the media, and positioned in the reactive site flow loop of a modified Chandler loop as described elsewhere[13-15]. Fresh whole blood (Blood Research Components, Cambridge, MA) was collected in a 10% acid/citrate dextrose solution (0.085 M trisodium citrate, 0.069 M citric acid, 0.111 M glucose, pH 4.6). Immediately before testing, a 0.1 M $CaCl_2$ and 0.075 M $MgCl_2$ solution was added to the blood (70-µL solution per 1 mL blood) and loaded into the flow loops. After 10 to 15-minute runs, the loops were emptied and flushed with 60 mL Tyrodes buffer (supplemented with 0.01 M HEPES, 0.75 M MgCl2) to remove non-adherent material. After visual assessment, the clot was lysed with 1% Triton-X solution for 20 minutes. Total erythrocyte content, a surrogate for clot formation that correlates with thrombus mass, was quantified through hemoglobin level (Quantichrome heme assay).

RIPA extraction and Western Blot analysis

Non-specific cell lysis was performed by rinsing cell-coated constructs twice with ice cold PBS and then incubating them for 30min on ice in RIPA buffer containing 50mM Tris-HCl, pH 7.4, 150mM NaCl, 1% NP-40, 0.5% sodium deoxycholate, 0.1% SDS and 5mM EDTA. The supernatant was extracted after centrifugation for 30min at 13,000g and 4ºC, and mixed with 1:4 v/v of Laemlli's buffer (Boston Bioproducts, Boston, MA) with 8% mercaptoethanol (Sigma). 10% acrylamide gels (Life Technologies) were used for protein separation. Gels were blotted using Life Technologies gel transfer stacks and blotting system. Membranes were blocked with 5%

powdered milk and incubated overnight at 4^0C while shaking with the antibodies of interest diluted at their optimal concentration. After two washes with PBS-T (PBS, 0.05% Tween20, Sigma), membranes were incubated with appropriate HRP-conjugated secondary antibodies diluted 1:2,000 for 1h while shaking at room temperature. After two 10 min washes in PBS-T, Luminata™ Forte Western HRP Substrate (Milipore, Billerica, MA) was applied and luminescence was detected in a Chemidoc XRS+ (Bio-Rad, Hercules, CA). Densitometry plots were analyzed using ImageJ (NIH, Washington, DC).

Microscopic examination

Cellular functionality within constructs was assessed using immunofluorescence (IF), scanning electron microscopy (SEM) and Hematoxylin & Elastin (H&E) staining. For IF, constructs were rinsed with PBS and fixed with 4% paraformaldehyde (PFA, Sigma) for 30 minutes at room temperature. Excessive aldehydes were quenched with 0.2M glycine in PBS for 10 minutes and, after washing with PBS, cells were permeabilized with 0.2% X-100 Triton in PBS for 10 minutes. After two consecutive washes with PBS for 10 minutes and 1 hour blotting with 5% goat serum in PBS-BSA (PBS, 1% bovine serum albumin, Sigma), cells were labeled overnight at 4^0C with their respective antibodies, diluted 1:50 in PBS-BSA. Cells were rinsed twice with PBS-BSA for 10 minutes and stained with the appropriate secondary antibodies and DAPI solution (1:100 in PBS-BSA) for 2h. Two additional 10 minutes washes with PBS were performed to remove any unbound antibody. Specimens were imaged using a Nikon (Tokyo, Japan) Eclipse TI-E epifluorescence microscope or a Perkin-Elmer (Waltham, MA) spinning disk confocal system coupled to a Zeiss (Jena, Germany) Axiovert 200M microscope. The list of antibodies used is detailed in a separate section in the supplemental methods.

For *ex vivo* detection of macrophage presence in atheroma plaques in carotid bifurcations from high-fat diet mice, multiphoton imaging was carried out as described previously[16]. The protocol was approved by the Massachusetts Institute of Technology Committee on Animal Care (protocol number 0412-032-15). Briefly, ten mice (12 weeks old) receiving a high-fat diet were anesthetized with isoflurane and injected into the tail vein with 200 µL of 20 mg/mL Texas Red-

70-kDa dextran in Dulbecco's PBS in order to load macrophages by phagocytosis 4 h before imaging. After 4 hours the animals were euthanized by overexposure to CO_2. Afterwards, left and right carotid were isolated and exposed. Fluorescent micro angiography was conducted after identifying both blood vessels and their bifurcations. Then, mice were perfused transcardially via the right and left ventricles with phosphate buffered saline (PBS) followed by an injection of fluorescein isothiocyanate-labeled 2,000 kDa dextran (FITC-dextran, Sigma). Finally, carotid fluorescence was visualized under a multiphoton microscope (Leica Microsystems, Heerbrugg, Switzerland). Macrophage pixel presence and intensity was determined by capturing z-series of carotid bifurcations labeled with Texas red-dextran, with a 25 x, N.a. 1.05 objective, Olympus FV-1000 MP (Olympus, Center Valley, PA) in which the viewing field is 512 × 512 µm.

For SEM, cells on constructs were first fixed in 3% glutaraldehyde, rinsed with PBS and subjected to a series of dehydration steps, which included 30 minutes incubations in ethanol solutions of increasing content in ethanol (50, 70, 95 and 100%) and 1 hour in acetone. Specimens were air dried overnight, sputter coated for 45 seconds using a Denton (Mooretown, NJ) Vacuum Desk II Sputter Coater and imaged with a Hitachi (Tokyo, Japan) S-3400N scanning electron microscope.

For H&E, cells on constructs were fixed in 4% PFA and subjected to a series of infiltration steps, which included 24 hour incubations in Spurr's resin (Electron Microscopy Sciences, Hatfield, PA) solutions in ethanol solutions of increasing content in Spurr's resin (25, 50, 75, 95, 100%). The resulting blocks were sampled and micro ground using an EXAKT 400CS Micro Grinding System (EXACT, Norderstedt, Germany) progressively until a 70-80 µm thickness. Samples were finally observed using an optical microscope.

Antibodies

For immunofluorescence, the primary antibodies used were rabbit polyclonal anti-CD31 (abcam, Cambridge, MA), mouse monoclonal anti-CD142 (Sekisui Diagnostics), mouse

monoclonal anti-α-smooth muscle cell actin (Sigma) and rabbit polyclonal anti-α-tubulin (Santa Cruz Biotechnology). The secondary antibodies used were Alexa Fluor® 647 goat anti-mouse IgG (H+L), Alexa Fluor® 568 goat anti-rabbit IgG (H+L) and Alexa Fluor® 647 goat anti-rabbit IgG (H+L), all by Life Technologies.

For western blot, the primary antibodies used were mouse monoclonal anti-CD106 (Santa Cruz Biotechnology Santa Cruz, CA) diluted 1:50, mouse monoclonal anti-α-tubulin (Cell Signaling, Danvers, MA) diluted 1:1,000, rabbit polyclonal anti-p-eNOS (Cell Signaling) diluted 1:250 and rabbit polyclonal anti-KLF-2 (abcam) diluted 1:100. The secondary antibodies used were HRP goat anti-mouse IgG (H+L) and HRP goat anti-rabbit IgG (H+L) by Bio-Rad.

SUPPLEMENTAL FIGURE LEGENDS

Figure S1. 2D Angiograms to define the curvature of the vessel

2D DICOM images (n=10) were combined to describe the curvature of the left main bifurcation to the left anterior descending and left circumflex coronary arteries. The images show the contrast injection observed from the LAO 60 atrio-ventricular (A) LAO 60 interventricular (B), RAO 30 atrio-ventricular (C) and RAO 30 interventricular planes (D).

Figure S2. Splines define the flow normal direction to define the tangential velocity

(A) Every node of each bifurcation was analyzed to determine its orientation relative to the spline that defines the direction of the arterial branch. (B) The dot product of the velocity vector at the node and the direction vector of the spline was defined as the node's tangential velocity (vTan). If the tangential velocity was negative, the tetrahedron was accounted as recirculating and included in the variable NVV.

Figure S3. Recirculation quantifier choice

(A) NVV was the metric found to better correlate flow recirculations with Ox-LDL uptake. Other parameters such as the total volume of recirculation (VolRec) and the percentage of volume of recirculation (%VolRec) at the peak of recirculation and their integrals along the pulse (Int VolRec, Int %VolRec) correlated worse than NVV. (B) The residence time of a particle in a recirculating streamline and the minimal tangential velocity on each branch showed the worse correlation.

Figure S4. Examples of immunofluorescence images

(A-C) Ox-LDL uptake by EC was measured by fluorescent quantification of Dil tag (red) and DAPI (blue). (D-F) Monocyte adhesion was evaluated by immunostaining against α-tubulin (red) and DAPI (blue). (G-I) TF in SMC was measured by immunostaining SMC against TF (red) and DAPI (blue). The data are expressed as a ratio of Alexa Fluor® 647 intensity divided by DAPI intensity.

Figure S5. Macrophage presence in murine carotid bifurcations

(A) Carotid bifurcations from male C57BL/6 mice (n=8), fed with a high-fat diet were stained with FITC-2,000kDa Dextran (green) for vessel identification and Texas Red-70kDa Dextran (red) for macrophage presence. Yellow, as a sum of red and green, shows macrophage presence. CFD simulations (B) allowed calculation a mapping of vTan showing how regions of flow stagnation (average vTan<200 mm/s) present higher macrophage recruitment *in vivo*.

Video S1. Vessel-like model of the carotid bifurcation

The video shows a cell-seeded mimic of the carotid bifurcation connected to the bioreactor. One can observe the pulsatility of the model due to the change of pressure from the peristaltic pump.

Table S1. Human bifurcation parameters

The table shows the geometrical and fluidodynamic parameters used to design the mimics of the human carotid and coronary bifurcations

SUPPLEMENTAL REFERENCES

1. Yasu T, Yamagishi M, Beppu S, Nagata S, Miyatake K. Left main coronary flow velocity associated with stenosis. Evaluation by transesophageal color-guided pulsed doppler technique. *Chest*. 1993;**104**:690-693
2. Kolachalama VB, Bressloff NW, Nair PB, Shearman CP. Predictive haemodynamics in a one-dimensional human carotid artery bifurcation. Part ii: Application to graft design. *IEEE Trans Biomed Eng*. 2008;**55**:1176-1184
3. Kolachalama VB, Bressloff NW, Nair PB. Mining data from hemodynamic simulations via bayesian emulation. *Biomed Eng Online*. 2007;**6**:47
4. Balcells M, Martorell J, Olive C, Santacana M, Chitalia V, Cardoso AA, Edelman ER. Smooth muscle cells orchestrate the endothelial cell response to flow and injury. *Circulation*. 2010;**121**:2192-2199
5. Tdyn. Http://www.Compassis.Com/compass/en/productos/tdyn. 02-12-2013
6. Windberger U, Bartholovitsch A, Plasenzotti R, Korak KJ, Heinze G. Whole blood viscosity, plasma viscosity and erythrocyte aggregation in nine mammalian species: Reference values and comparison of data. *Exp Physiol*. 2003;**88**:431-440
7. Hartley CJ, Taffet GE, Reddy AK, Entman ML, Michael LH. Noninvasive cardiovascular phenotyping in mice. *ILAR J*. 2002;**43**:147-158
8. Davies PF, Civelek M, Fang Y, Fleming I. The atherosusceptible endothelium: Endothelial phenotypes in complex haemodynamic shear stress regions in vivo. *Cardiovasc Res*. 2013;**99**:315-327
9. Dai G, Kaazempur-Mofrad MR, Natarajan S, Zhang Y, Vaughn S, Blackman BR, Kamm RD, Garcia-Cardena G, Gimbrone MA, Jr. Distinct endothelial phenotypes evoked by arterial waveforms derived from atherosclerosis-susceptible and -resistant regions of human vasculature. *Proc Natl Acad Sci U S A*. 2004;**101**:14871-14876
10. Zarins CK, Giddens DP, Bharadvaj BK, Sottiurai VS, Mabon RF, Glagov S. Carotid bifurcation atherosclerosis. Quantitative correlation of plaque localization with flow velocity profiles and wall shear stress. *Circ Res*. 1983;**53**:502-514
11. Methe H, Balcells M, Alegret Mdel C, Santacana M, Molins B, Hamik A, Jain MK, Edelman ER. Vascular bed origin dictates flow pattern regulation of endothelial adhesion molecule expression. *Am J Physiol Heart Circ Physiol*. 2007;**292**:H2167-2175
12. Schubert SY, Benarroch A, Monter-Solans J, Edelman ER. Primary monocytes regulate endothelial cell survival through secretion of angiopoietin-1 and activation of endothelial tie2. *Arterioscler Thromb Vasc Biol*. 2011;**31**:870-875
13. Kolandaivelu K, Edelman ER. Low background, pulsatile, in vitro flow circuit for modeling coronary implant thrombosis. *J Biomech Eng*. 2002;**124**:662-668
14. Kolandaivelu K, Swaminathan R, Gibson WJ, Kolachalama VB, Nguyen-Ehrenreich KL, Giddings VL, Coleman L, Wong GK, Edelman ER. Stent thrombogenicity early in high-risk interventional settings is driven by stent design and deployment and protected by polymer-drug coatings. *Circulation*. 2011;**123**:1400-1409
15. Chitalia VC, Shivanna S, Martorell J, Balcells M, Bosch I, Kolandaivelu K, Edelman ER. Uremic serum and solutes increase post-vascular interventional thrombotic risk through altered stability of smooth muscle cell tissue factor. *Circulation*. 2013;**127**:365-376
16. Wyckoff JB, Wang Y, Lin EY, Li JF, Goswami S, Stanley ER, Segall JE, Pollard JW, Condeelis J. Direct visualization of macrophage-assisted tumor cell intravasation in mammary tumors. *Cancer Res*. 2007;**67**:2649-2656

Figure S1

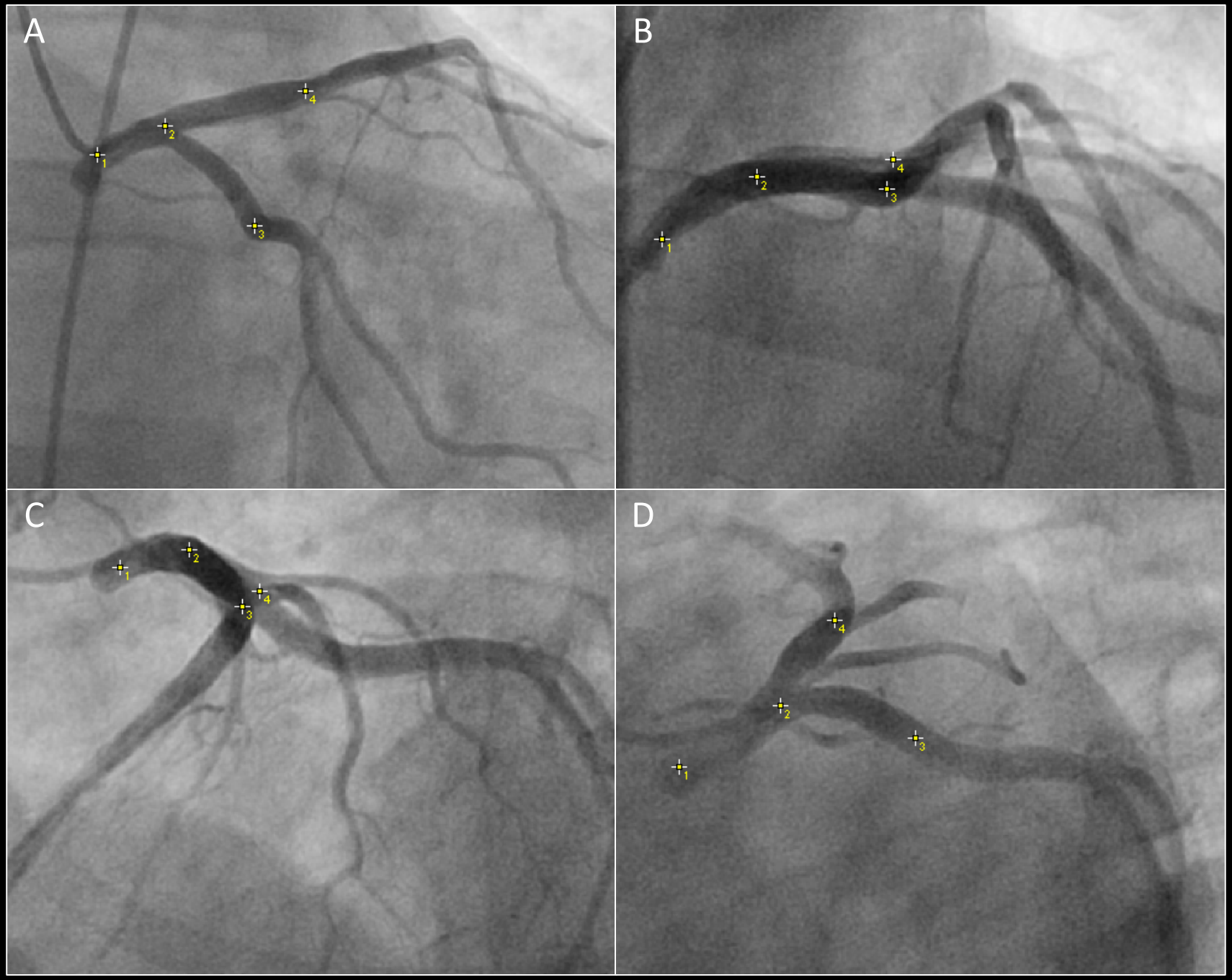
A
B
C
D

Figure S2

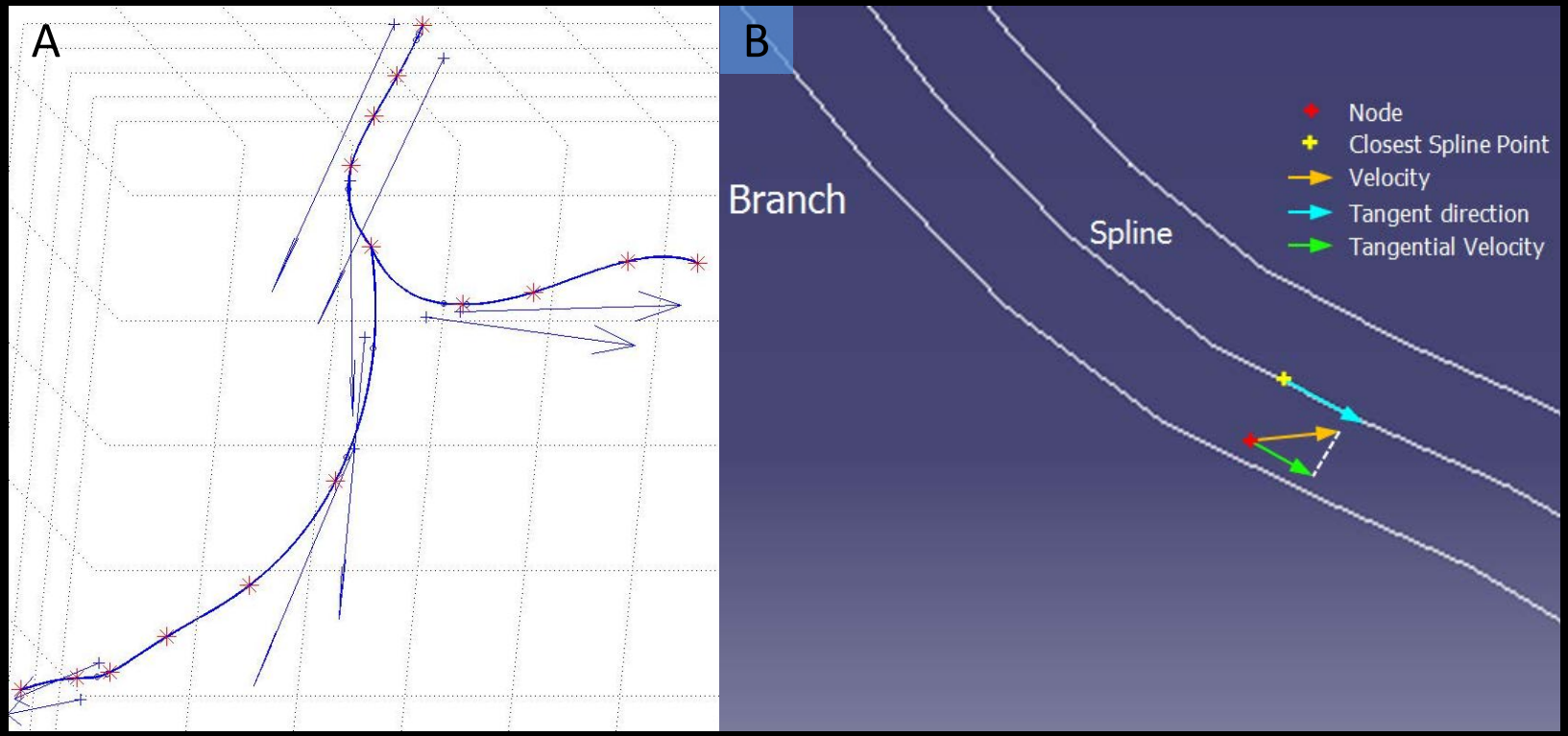
A
B
Branch
Spline
Node
Closest Spline Point
Velocity
Tangent direction
Tangential Velocity

Figure S3

A

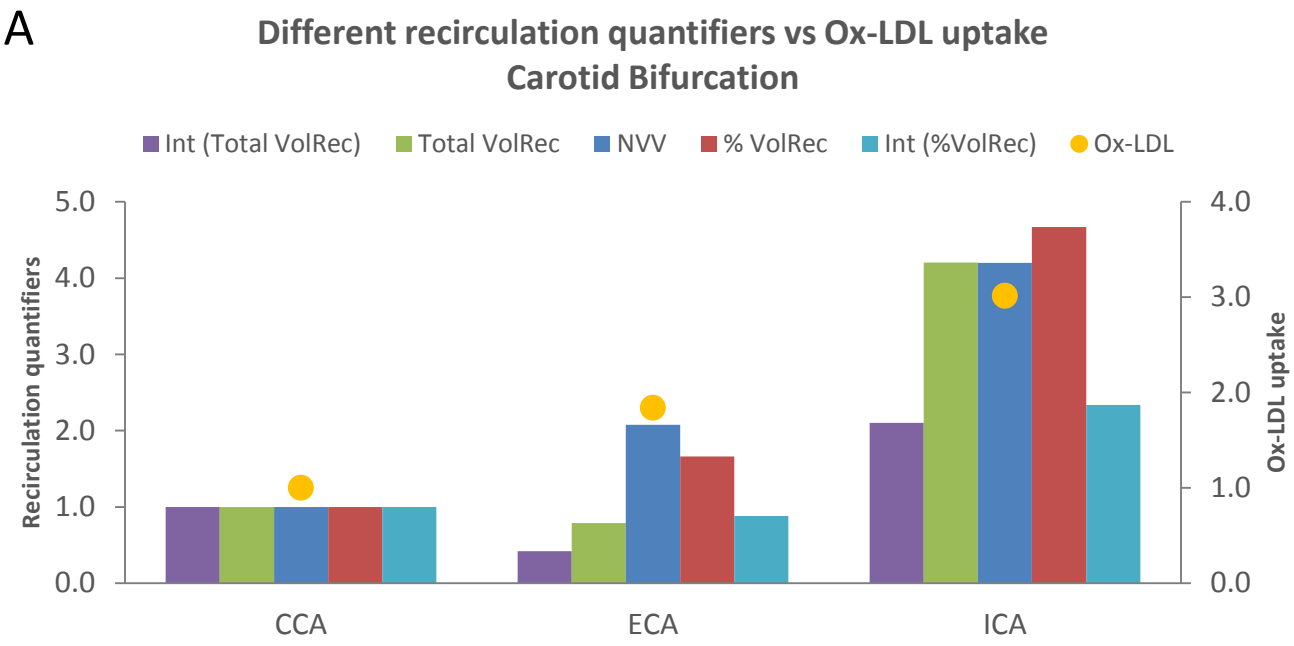
Different recirculation quantifiers vs Ox-LDL uptake
Carotid Bifurcation
Int (Total VolRec)
Total VolRec
NVV
% VolRec
Int (%VolRec)
Ox-LDL
Recirculation quantifiers
Ox-LDL uptake
5.0
4.0
3.0
2.0
1.0
0.0
CCA
ECA
ICA

B

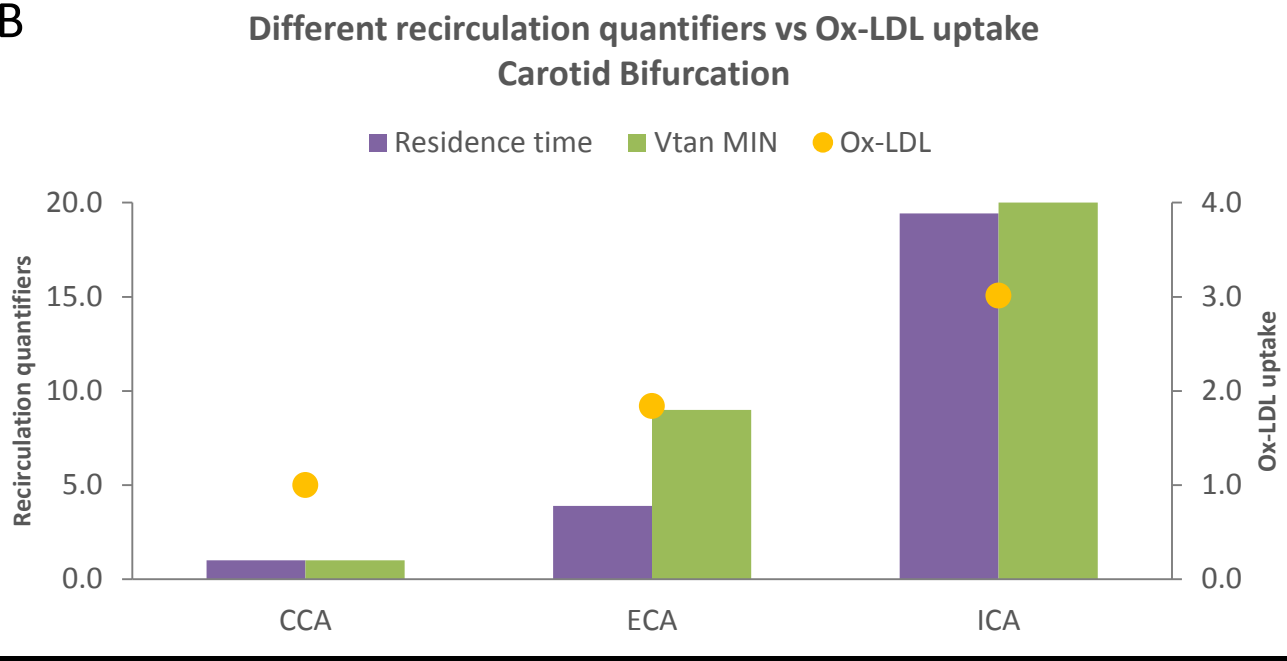
Different recirculation quantifiers vs Ox-LDL uptake
Carotid Bifurcation
Residence time
Vtan MIN
Ox-LDL
Recirculation quantifiers
Ox-LDL uptake
20.0
15.0
10.0
5.0
0.0
4.0
3.0
2.0
1.0
0.0
CCA
ECA
ICA

Figure S4

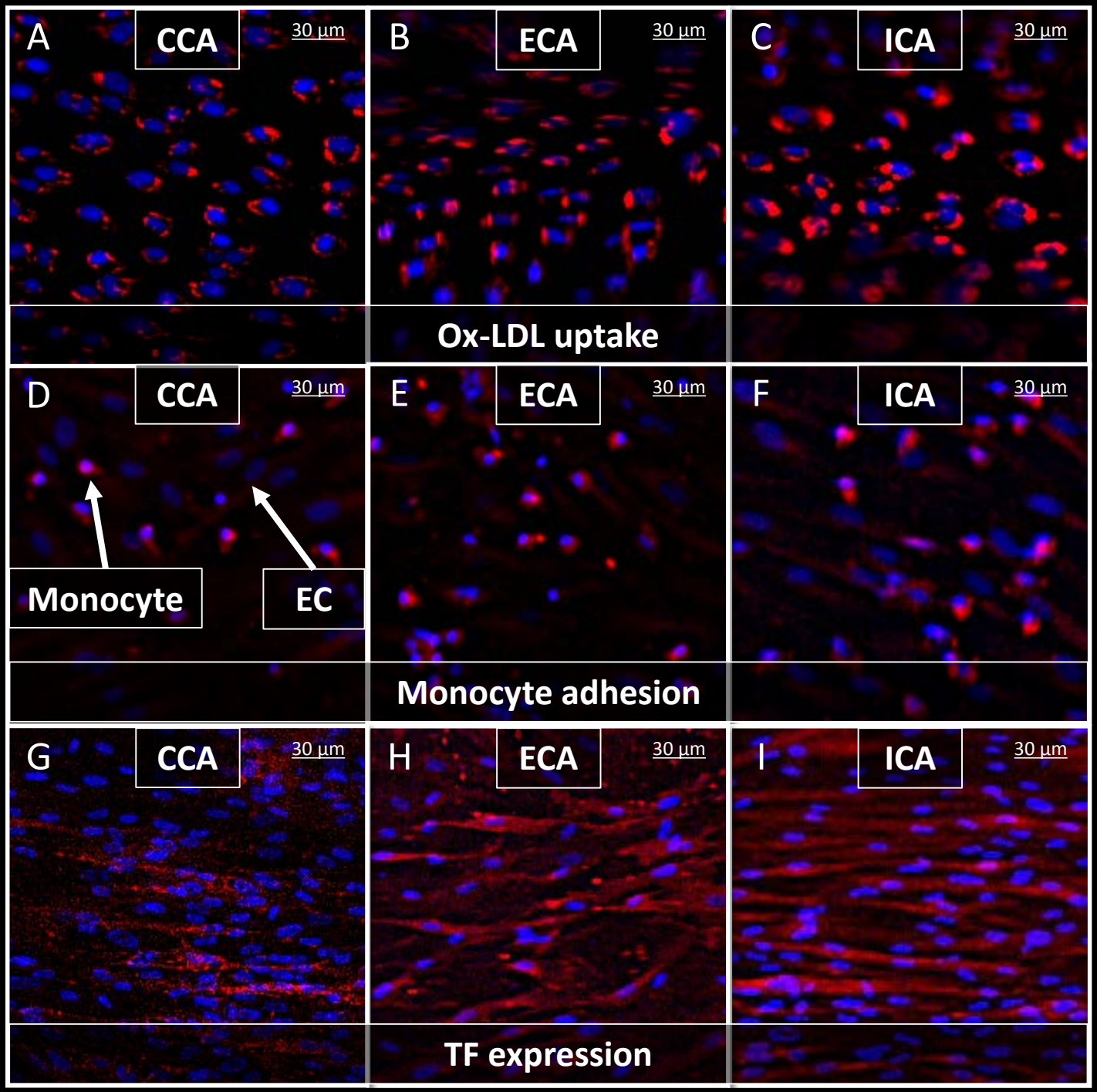
A
CCA
30 µm
B
ECA
30 µm
C
ICA
30 µm
Ox-LDL uptake
D
CCA
30 µm
Monocyte
EC
E
ECA
30 µm
F
ICA
30 µm
Monocyte adhesion
G
CCA
30 µm
H
ECA
30 µm
I
ICA
30 µm
TF expression

Figure S5

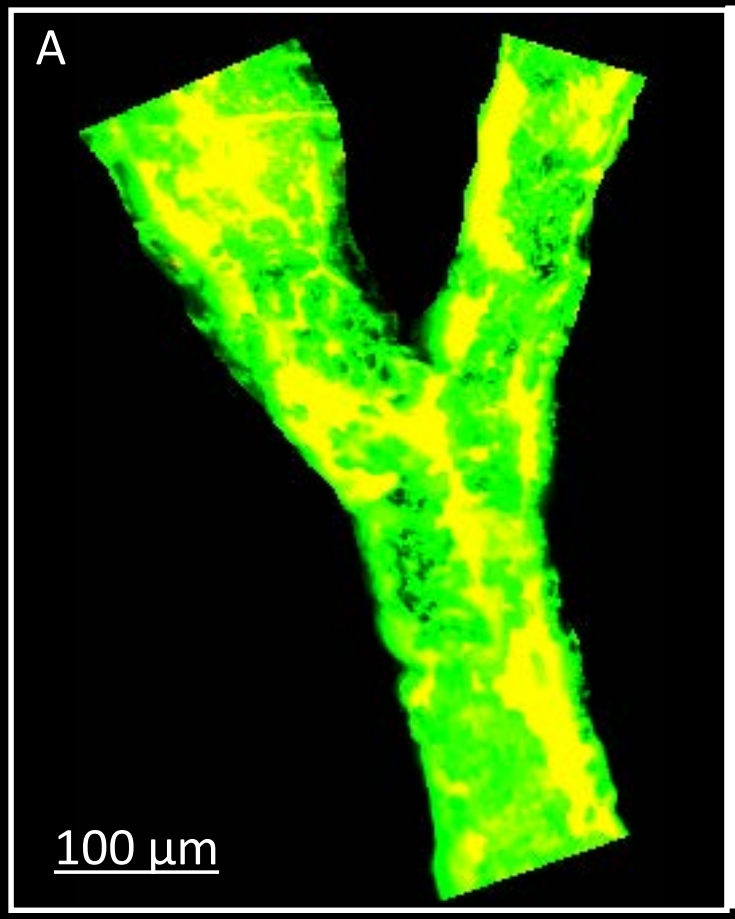
A
100 µm

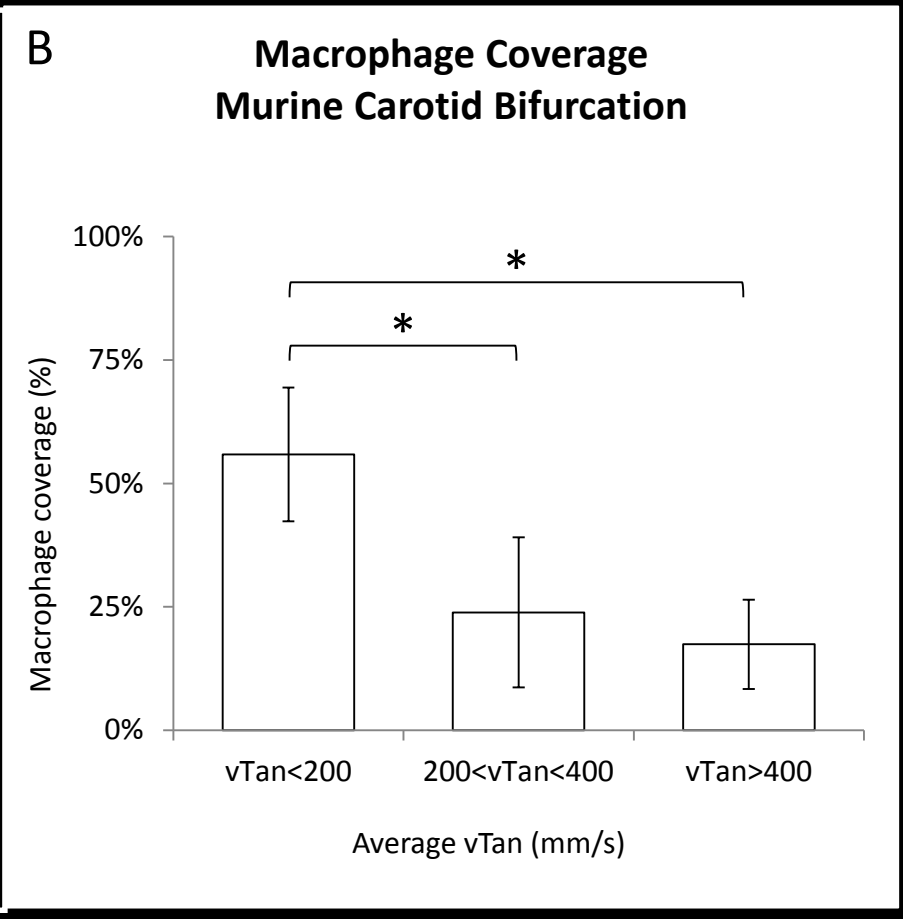
B
Macrophage Coverage
Murine Carotid Bifurcation
100%
75%
50%
25%
0%
Macrophage coverage (%)
*
*
vTan<200
200<vTan<400
vTan>400
Average vTan (mm/s)

Video S1


SMC

Table S1

Carotid bifurcation		
Section	Length (mm)	Width (mm)
CCA 1	8.0	8.0
CCA 2	16.0	8.0
CCA 3	32.0	8.0
ICA 1	0.0	8.3
ICA 2	7.3	8.9
ICA 3	14.5	8.2
ICA 4	24.0	5.7
ECA 1	0.0	5.6
ECA 2	10.0	5.5
ECA 3	15.0	4.6
ECA Angle (º)	25.10	
ICA Angle (º)	25.40	
Inlet velocity (m/s)	0.7	

Idealized coronary bifurcation		
Section	Length (mm)	Width (mm)
LM 1	4.0	3.8
LM 2	20.0	3.6
LAD 1	0.0	2.8
LAD 2	16.0	2.8
LCX 1	0.00	2.7
LCX 2	14.0	2.7
LAD Angle (º)	31.5	
LCX Angle (º)	31.5	
Inlet velocity (m/s)	0.35	